Title: Vitamin D constrains inflammation by modulating the expression of key genes on Chr17q12-21.1

Authors: Ayşe Kılıç[1*], Arda Halu[1*#], Margherita De Marzio[1,2], Enrico Maiorino[1], Melody G. Duvall[3], Thayse Brueggemann[3], Joselyn J. Rojas Quintero[3], Robert Chase[1], Hooman Mirzakhani[1], Ayse Özge Sungur[4, 5], Janine Koepke[5], Taiji Nakano[6], Hong Yong Peh[3], Nandini Krishnamoorthy[3], Raja-Elie Abdulnour[3], Katia Georgopoulos[7], Augusto A. Litonjua[8], Marie B. Demay[9], Harald Renz[10,11], Bruce D. Levy[3] and Scott T. Weiss[1*#]

Affiliations:

[1] Channing Division of Network Medicine, Department of Medicine, Brigham and Women's Hospital and Harvard Medical School; Boston, MA, USA.

[2] Department of Environmental Health, Harvard TH Chan School of Public Health; Boston, MA, USA.

[3] Division of Pulmonary and Critical Care Medicine, Department of Medicine, Brigham and Women's Hospital and Harvard Medical School; Boston, MA, USA.

[4] Behavioral Neuroscience, Experimental and Biological Psychology, Philipps-University Marburg; Marburg, Germany.

[5] Excellence Cluster Cardio-Pulmonary System (ECCPS), Justus Liebig University Giessen; Giessen, Germany.

[6] Department of Pediatrics, Graduate School of Medicine, Chiba University; Chiba, Japan.

21 [7] Cutaneous Biology Research Center, Massachusetts General Hospital and Harvard Medical
22 School; Charlestown, Massachusetts, USA.

23 [8] Division of Pediatric Pulmonary Medicine, Golisano Children's Hospital at Strong, University
24 of Rochester Medical Center; Rochester, NY, USA.

25 [9] Endocrine Unit, Massachusetts General Hospital and Harvard Medical School; Boston, MA,
26 USA.

27 [10] Institute of Laboratory Medicine and Pathobiochemistry, Molecular Diagnostics, Philipps
28 University of Marburg and German Center for Lung Research (DZL); Marburg, Germany.

29 [11] Department of Clinical Immunology and Allergology, Laboratory of Immunopathology
30 Sechenov University; Moscow, Russia.

31 *These authors contributed equally to the manuscript.

32 #Corresponding author. Arda Halu (rehal@channing.harvard.edu), Scott T. Weiss
33 (restw@channing.harvard.edu)

34

35

36

37

38 **Abstract:** Vitamin D possesses immunomodulatory functions and vitamin D deficiency has been
39 associated with the rise in chronic inflammatory diseases, including asthma (1). Vitamin D
40 supplementation studies do not provide insight into the molecular genetic mechanisms of vitamin
41 D mediated immunoregulation. Here we provide evidence for vitamin D regulation of two human

chromosomal loci, Chr17q12-21.1 and Chr17q21.2, reliably associated with autoimmune and chronic inflammatory diseases (2–4). We demonstrate increased vitamin D receptor (VDR) expression in mouse lung CD4+ Th2 cells, differential expression of Chr17q12-21.1 and Chr17q21.2 genes in Th2 cells based on vitamin D status and identify the IL-2/Stat5 pathway as a target of vitamin D signaling. Vitamin D deficiency caused severe lung inflammation after allergen challenge in mice that was prevented by long term prenatal vitamin D supplementation. Mechanistically, vitamin D induced the expression of the *Ikzf3* encoded protein Aiolos to suppress IL-2- signaling and ameliorate cytokine production in Th2 cells. These translational findings demonstrate mechanisms for the immune protective effect of vitamin D in allergic lung inflammation with a strong molecular genetic link to the regulation of both Chr17q12-21.1 and Chr17q21.2 genes and suggest further functional studies and interventional strategies for long-term prevention of asthma and other autoimmune disorders.

One Sentence Summary: Vitamin D regulates two human chromosomal loci, Chr17q12-21.1 and Chr17q21.2, that are associated with autoimmune and chronic inflammatory diseases.

INTRODUCTION

The vitamin D receptor was genetically associated with asthma in 2004 (5) and high intake of vitamin D by pregnant women is associated with about a 50% reduction in asthma risk in the mother's offspring (6,7). Together, these findings led to a comprehensive theory about how vitamin D deficiency could influence asthma occurrence through its effects on lung and immune system development and that progressive decreases in vitamin D intake from 1946 onward could be contributing to the epidemic of allergic and autoimmune diseases (1). Vitamin D deficiency is

64 the most common vitamin deficiency in the world today and is particularly prevalent in pregnant
65 women where the fetal lung and immune system are developing in utero (8–10).

66 To determine the impact of vitamin D supplementation, we have previously performed a clinical
67 trial, the Vitamin D Antenatal Asthma Trial (VDAART) in pregnant women who either had
68 allergies or asthma or had family members with these conditions. The participants were given
69 either 4400 IU of vitamin D3 or 400 IU and were followed throughout their pregnancy and for the
70 first six years of the life of the child (11). The results of the trial were not statistically significant
71 using conventional intent to treat analysis (12,13) but the reasons were complex, as is often seen
72 when the effects of nutrients are studied. Most importantly, unlike conventional drug trials where
73 one compares drug to no drug or alternative drug, in nutrient trials there is nutrient already present
74 in the placebo group. This creates misclassification that can reduce trial power. When we
75 performed a meta-analysis of the two pregnancy related trials of vitamin D, we got a statistically
76 significant reduction in asthma in the offspring of women who had the higher vitamin D intake
77 during pregnancy and, when we adjusted for the baseline level of vitamin D in the meta-analysis,
78 we got a reduction in asthma risk of 50 percent, exactly what we saw in the observational studies
79 performed previously (14,15).

80 To link the results of the VDAART trial directly to the chr17q12 locus, our group then genotyped
81 the single nucleotide polymorphism (SNP) rs12936231, located in ZPBP2, the gene adjacent to
82 ORMDL3, and stratified the VDAART trial results by maternal genotype at this locus. This study
83 found that the vitamin D effect in the trial was significantly influenced by genotype, with the GG
84 genotype exhibiting a protective effect on asthma risk in the child and the CC or GC genotype not
85 being responsive to vitamin D; additionally this result was related to sphingolipid production with
86 the children protected from asthma having higher sphingolipid production (3).

87 This SNP (rs12936231) is one of two SNPs (the other being rs4065275) that alter the chromatin
88 state of a regulatory domain, specifically two CTCF binding sites, in the chr17q12-21.1 locus that
89 are correlated with the expression of ORMDL3 (4,16). 4C-seq assays previously demonstrated that
90 the ORMDL3 promoter interacts with a long-range enhancer in IKZF3 that promotes (or represses)
91 transcription of ORMDL3 in cells expressing both genes and the binding of CTCF per the G allele
92 of rs12936231 in ZPBP2 blocks this interaction, resulting in reduced transcription of ORMDL3
93 on haplotypes with the rs12936231-G allele (4). If rs12936231 is not activated, then there is
94 activation of the other CTCF binding site (rs4065275) intronic to ORMDL3, thus favoring the
95 expression of ORMDL3 and increased asthma risk (4).

96 Mouse models have contributed to our understanding of ORMDL3 function as mice expressing
97 the ORMDL3 transgene exhibit spontaneous increases in airway hyper responsiveness (AHR), the
98 essential feature of asthma. This increase in AHR was associated with airway remodeling and peri
99 bronchial fibrosis without airway inflammation (17). ORMDL3 is pleotropic, influencing Ca++
100 signaling, and the unfolded protein response. Most importantly, increased expression of ORMDL3
101 inhibits the enzyme serine palmityl-transferase, the rate limiting step in the production of
102 sphingolipids, and ORMDL3 transgenic mice have reduced levels of sphingolipids (18). What has
103 been unclear so far is how ORMDL3 is controlled.

104 In the current manuscript we provide evidence for vitamin D regulation of two human
105 chromosomal loci, Chr17q12-21.1 and Chr17q21.2, reliably associated with autoimmune and
106 chronic inflammatory diseases. We demonstrate increased vitamin D receptor (VDR) expression
107 in mouse lung CD4+ Th2 cells, differential expression of these Chr17q12-21.1 and Chr17q21.2
108 genes in Th2 cells based on vitamin D status and identify the IL-2/Stat5 pathway as a target of
109 vitamin D signaling. Vitamin D induced the expression of the *Ikzf3* encoded protein Aiolos to

110 suppress IL-2- signaling and ameliorate cytokine production in Th2 cells thus demonstrating a
111 mechanism for how vitamin D influences autoimmunity.

112

113 **MATERIALS AND METHODS**

114 ***In silico analysis of VDR binding sites on Chr17q12-21***

115 For our *in-silico* analysis, we focused on two genomic regions that are known to harbor variants
116 associated with asthma and autoimmune disease susceptibility. The first one is a 240 kb region
117 that covers parts of the 17q12 and 17q21.1 loci and contains IKZF3, ZPBP2, ORMDL3, GSDMA
118 and GSDMB (chr17: 37,899,254–38,139,253; hg19) and the second one is a 420 kb region in the
119 17q21.2 locus that includes STAT3, STAT5A and STAT5B (chr17: 40,330,000-40,750,000;
120 hg19). When selecting these genomic ranges, our criterion was to make the window inclusive of
121 any potential enhancer regions targeting the above genes of interest. We used the GeneHancer (19)
122 track in the UCSC Genome Browser (http://genome.ucsc.edu) to determine predicted enhancer-
123 target gene interactions. We obtained VDR, IKZF3, CTCF and Vitamin D-sensitive CTCF binding
124 sites from (20–23), converted their genomic coordinates to hg19 if a different genome build was
125 used in the original publication, and added them as custom tracks on the Genome Browser. We
126 retrieved the known disease and trait associations in these loci from the NHGRI-EBI GWAS
127 Catalog (downloaded on 7/26/2021) (24) and retained all hits that were deemed significant ($p<10^{-}$
128 ^{5}). We downloaded significant single-tissue eQTLs for IKZF3 and PSMCIP3 in all tissues from
129 the Common Fund (CF) Genotype-Tissue Expression Project (GTEx) Analysis Release V8
130 (dbGaP Accession phs000424.v8.p2), through the GTEx Portal
131 (https://www.gtexportal.org/home/) in July 2021. We calculated linkage disequilibrium (LD)

132 using the NCI LDmatrix Tool (https://ldlink.nci.nih.gov/?tab=ldmatrix), and by selecting all
133 available populations.

134 ***The Vitamin D Antenatal Asthma Trial (VDAART)***

135 The design, eligibility and initial results of the trial have been published (11–17). Pregnant
136 women were recruited from 3 clinical sites across the United States – Boston Medical Center,
137 Boston, MA; Washington University at St. Louis, St. Louis, MO; and Kaiser Permanente
138 Southern California Region, San Diego, CA. The Data Coordinating Center was based in the
139 Channing Division of Network Medicine, Brigham and Women's Hospital, Boston, MA.
140 Eligible participants were women between the ages of 18 and 39 years, who presented between
141 the estimated gestational ages of 10 and 18 weeks; who had a history of asthma, eczema, or
142 allergic rhinitis, or whose partner (biologic father of the child) had a history of asthma, eczema,
143 or allergic rhinitis; who was a non-smoker; and who was English- or Spanish- speaking, with
144 intent to participate for 4 years (up to the 3rd birthday of the child). The VDAART study protocol
145 was approved by the institutional review boards at each participating institution and at the
146 Brigham and Women's Hospital. All women provided a written informed consent. The trial was
147 registered with clinical trials.gov: clinicaltrials.gov Identifier: NCT00920621.

148

149 ***Gene expression analysis in VDAART cohort***

150 To understand the putative mechanism linking IKZF3 expression and Vitamin D to asthma risk
151 we considered umbilical cord blood (CB) RNA-seq data from the VDAART trial. **Figure 1-figure**
152 **supplement 1*C*** shows the study design. Total RNA was isolated from cord blood using the
153 QIAGEN PAXgene Blood RNA Kit (Qiagen) according to the manufacturer's protocol. Quality
154 was assessed using the Nanodrop 8000 spectrophotometer (ThermoFisher Scientific). Sequencing

155 libraries were constructed with the TruSeq® Stranded Total RNA Library Prep Globin Kit
156 (Illumina) and the NEXTflex Small RNA sequencing Kit v3 (Boo Scientific). Sequencing was
157 performed using a NextSeq 550 instrument (Illumina). Trimmed reads were mapped to The
158 GRCh38 reference genome using STAR (25). Read counts were computed with htseq (26). The
159 data includes 443 expression profiles of pregnant women with and without asthma undergoing
160 measurements of Vitamin D levels in their CB. Each sample is matched with the observed patterns
161 of wheezing and asthma in the newborn. We filtered all the samples where information about
162 Vitamin D levels, asthma/wheezing patterns or other covariates were missing, obtaining 393
163 expression profiles. Data was normalized with the voom function of the edgeR R package (27),
164 and Vitamin D levels were binarized using 30 ng/ml as threshold. We performed logistic regression
165 of asthma status as a function of the expression levels of IKZF1 and IKZF3, including their
166 interaction term and the interaction between IKZF3 and Vitamin D. Since IKZF3 forms
167 homodimers and heterodimers with IKZF1, we included IKZF1 in the model. We adjusted the
168 model for maternal asthma status and child race.

169 ***Mice***

170 All animal studies were approved by the institutional animal care committee. Mice were
171 maintained in a virus- and parasite-free animal facility under a 12-h light, 12-h dark cycle.
172 C57BL6/J wild type (WT) mice were bred and housed at the MGH animal facility. Vitamin D-
173 deficient mice (C57BL6/J) were bred and maintained in a UV-free environment and weaned onto
174 a similar diet lacking vitamin D metabolites (TD97340; Harlan Teklad) that results in undetectable
175 circulating 25-hydroxyvitamin D levels (28). $VDR^{-/-}$ mice ($Vd^{rtm1Mbd/J}$), on C57BL6/J background,
176 were bred and housed at the MGH animal facility, weaned at 18 d on a diet that maintains normal
177 mineral ion homeostasis in the absence of VDR signaling (2% calcium, 1.25% phosphorus, 20%

178 lactose supplemented diet, TD96348; Harlan Teklad, Madison WI) (29). BALB/c male and female
179 mice were purchased from Charles River Laboratories at 6–8 weeks of age and fed with diets
180 supplemented with varying amounts of vitamin-D3 (TD97340 was used as base diet and
181 supplemented with either 400 IU vitamin D/kg, 1000 IU vitamin D/kg or 4000 IU vitamin D/kg).
182 Mice were bred on the specific diets for two generations to assure stabilization of vitamin D levels.
183 Resulting F2 litters were used for the experiments. Mice were housed under standard conditions
184 with free access to rodent chow and water. All animal experiments were carried out in accordance
185 with NIH Guidelines for the Care and Use of Laboratory Animals as well as guidelines prescribed
186 by the Institutional Animal Care and Use Committee (IACUC) at Brigham and Women's Hospital
187 (2016N000357), Massachusetts General Hospital (2004N000113) and Harvard Medical Area
188 (05115) (AAALAC 1729).

189 ***House dust mite induced-airway inflammation***

190 Mice were exposed to D. pteronyssinus extracts (Greer Laboratories, 10.52 EU/mg endotoxin) via
191 the intranasal application of HDM (25 μg in saline) on days 1,2,3, 8 to 15. Control mice received
192 equal volumes of saline (Hospira Inc., Lake Forest, IL, USA). Twenty-four hours after the final
193 challenge, mice were sacrificed, and specimens sampled.

194 ***Bronchoalveolar Lavage***

195 Bronchoalveolar Lavage (BAL) was performed with 2 × 1 mL of PBS/0.02% bovine serum
196 albumin (BSA). The total number of leukocytes was determined using a TC20 Automated Cell
197 Counter (BioRad Systems). To differentiate cell types, cytospins were prepared and stained with
198 Kwik-Diff solutions as per manufacturer's instructions (Fisher Scientific) and 200 immune cells
199 per slide were counted.

200 ***Histological staining***

201 Lungs were perfusion fixed with zinc fixative (BD Pharmingen, San Diego, CA) Tissues were
202 paraffin embedded, divided into sections, and stained with hematoxylin and eosin by MGH
203 DF/HCC Specialized Histopathology Services Core Histology Core. After paraffin embedment, 3-
204 µm sections were stained with hematoxylin and eosin.

205 ***Measurements of serum immunoglobulins***

206 Blood samples were collected 24 hours after the final aerosol challenge and serum was prepared.
207 Total IgE levels were measured by ELISA (Chondrex) according to manufacturer's instructions.

208 ***Dissociation of mouse tissues, in vitro polarization of CD4 Th-subsets and flow cytometry***
209 ***analyses***

210 Lungs were perfused via the right heart ventricle with PBS, excised, and digested with collagenase
211 D (2 mg/ml; Roche) in RPM 1640 (Sigma-Aldrich) for 30 minutes at 37°C. The cell suspension
212 was washed twice with PBS. Erythrocytes were removed by hypotonic lysis. Cells were washed
213 twice with PBS and sieved with 30-µm cell strainers (Miltenyi Biotec). The resulting single cells
214 suspension was used to detect leukocyte populations (CD45 BV421 [clone: 104; Biolegend], CD4
215 PerCPeFluor710 [RM4-5; eBioscience], CD8a APC-Cy7 [53-6.7; Biolegend], CD19 PE-Cy7
216 [6D5; Biolegend]) and CD4+ Foxp3+ Treg (CD45 BV421, CD4 PerCPeFluor710, Foxp3 PE [FJK-
217 16s; Thermo Fisher]), VDR AlexaFluor647 (D2K6W; Cell Signaling Technologies), Aiolos PE
218 (8B2; Biolegend) and cytokine production by Th-cells (see below). Spleens were excised and
219 mononuclear cells were isolated using a syringe plunger and 100-µm cell strainers. Red blood cells
220 were removed by hypotonic lysis. Tonicity was restored by the addition of RPMI 1640 (Sigma
221 Aldrich). The resulting cell suspension was washed twice with PBS and used for the isolation of

222 naïve CD4+ T cells according to the manufacturer's instructions (Naive T Cell Isolation Kit II;
223 Miltenyi Biotec). Naive CD4+ T cell purity was assessed by staining for CD4 PerCPeFluor710
224 (clone: RM4-5), CD44 FITC (IM7), and CD62L PE (mel-14). Naïve T cells were activated with
225 plate bound anti-CD3ε (5 μg/ml, clone: 145-2C11, BD Biosciences) and soluble anti-CD28 (0.5
226 μg/ml, clone: 37.51, BD Biosciences). Th-subset polarization was induced by exposing naïve
227 CD4+Tcells to following culture conditions for 3 days. Th1 cells: recombinant murine IL-12
228 (rmIL-12) (10 ng/mL; Peprotech), anti–IL-4 (5 μg/mL; BD Biosciences); Th2 cells: rmIL-4 (20
229 ng/mL; Peprotech), anti–IFN-γ (5 μg/mL; BD Biosciences), and anti–IL-12 (5 μg/mL; BD
230 Biosciences); Treg: rmTGFβ1 (2 ng/mL; Peprotech), anti–IL-4 (5 μg/mL), anti–IFN-γ (5 μg/mL)
231 for 3 days. Proliferation of Th1 and Th2 cells was induced using rmIL-2 (20 ng/mL; Peprotech) in
232 the presence of Th-polarizing reagents for an additional 2 days. Polarization efficiency was
233 verified by staining for intracellular cytokines (please see below) or Foxp3 expression (see above).

234 For intracellular cytokine staining, cells were stimulated with phorbol 12-myristate 13-acetate
235 (PMA)/ionomycin and brefeldin A (Cell Stimulation Cocktail; Tonbo Biosiences) for 4 hours.
236 Cells were fixed with Fixation Buffer (Biolegend). Cells were permeabilized using 0.3% saponin
237 in FACS buffer (0.5% FBS in PBS). Antibody staining was performed for 30 minutes in the dark
238 using CD4, IFN-γ (XMG1.2-FITC), IL-10 (JES5-16E3-PE), IL-13 (eBio13A-eFluor660), IL-17A
239 (TC11-18H10.1-PE-Cy7). Cells were washed twice with permeabilization buffer and suspended
240 in FACS buffer. For analysis, 30,000 counts (in the CD4+ gate) were recorded on a FACSFortessa
241 (BD Biosciences) and analyzed with FlowJo software (v10; Tree Star).

242 ***Western blot analyses***

243 Cells were lysed in 50 mmol/L Tris/HCl (pH 7.5), 150 mmol/L NaCl, 1% NP-40, and 1× protease
244 and phosphatase inhibitor mix (both Roche) for 15 minutes on ice. Lysates were clarified, and total

245 protein concentrations were measured with BCA (Pierce). Proteins (20 µg) were separated on
246 gradient gels (Mini-PROTEAN® TGX; BioRad) and transferred on a Immun-Blot PVDF
247 membrane (BioRad). Unspecific binding was blocked using 5 % milk powder in TBST for 30 min.
248 Anti-VDR (D2K6W, 1:1000; Cell Signaling Technologies, CST) was incubated in 0.5 % milk
249 powder in TBST overnight at 4° C. Membranes were washed 3 times with TBST and incubated
250 with secondary anti-rabbit IgG, HRP-linked Antibody (#7074; CST) for 2 hours. To control for
251 equal loading, membranes was probed for β-actin (AC-15; 1:10,000; Sigma-Aldrich) expression
252 for 2 hrs. at RT. Protein bands were visualized with Luminol reagent (Pierce) using the ChemiDoc
253 XRS+system (BioRad).

254 ***Immunofluorescence staining for confocal microscopy***

255 *In vitro* polarized Th2 cells (see above) were stimulated with 100 nm calcitriol (in ethanol) or
256 ethanol [equal v/v] for the final 24 hours of culture. Cells were washed twice with PBS and spun
257 onto poly-L-lysine coated glass slides. After drying, cells were fixed with 4 % PFA in PBS for 15
258 min. Cells were permeabilized using 0.2% Triton X-100 in PBS for 20 min. Cells were washed 3
259 times for 5 min with PBS and incubated with Image-iT FX Signal Enhancer (Thermo Fisher
260 Scientific) for 30 min at RT. After three consecutive washes with PBS, unspecific binding was
261 blocked using blocking buffer (PBS/5 % goat serum/0.3 % Triton X-100) for 60 min at RT.
262 Primary antibodies directed against CD4-FITC (clone; 1:100, BD Biosciences), VDR (D2K6W;
263 1: 200, CST) were incubated in a humidified chamber over night at 4° C. After 3 washes with PBS,
264 slides were incubated with the secondary reagent, anti-rabbit-Cy3 (1:500; Thermo) for 30 min at
265 RT in the dark. After three more washes with PBS, slides were mounted with ProLong Gold with
266 DAPI according to manufacturer's instructions (Invitrogen). Images were acquired in a single z-
267 plane using a Zeiss immunofluorescence microscope with a 40x objective.

268 ***Total RNA isolation, quality control, and RNA-sequencing analysis***

269 Total RNA was isolated using TRIzol™ Reagent (Invitrogen) according to the manufacturer's
270 instructions. Quality was assessed using the Nanodrop 8000 spectrophotometer. Sequencing
271 libraries were constructed with the TruSeq® Stranded Total RNA Library Prep Globin Kit
272 (Illumina). Sequencing was performed using a HiSeq. 2500 instrument (Illumina). Trimmed reads
273 were mapped to the GRCm38 reference genome using STAR (25). Read counts were computed
274 with htseq (26). Data were normalized and differential expression was analyzed with the R package
275 DESeq2 (v.1.34.0)(30) using a false discovery rate (FDR) < 0.05.

276 ***Pathway enrichment, Overrepresentation and Gene Set Enrichment analysis***

277 KEGG pathway, overrepresentation and gene set enrichment analyses were performed with the
278 "enrichKEGG", "enrichr" and "GSEA" function in the R package "clusterProfiler" (v.3.10.1) with
279 default settings(31). P-values were adjusted using the BH-FDR correction and enriched terms with
280 a p-adj.<0.05 selected.

281 ***Network analysis in the mice***

282 RNA-Sequencing data extracted from murine Th2 cells were analyzed using the R package
283 DESeq2 (v.1.22.2) (30). Raw counts were normalized and transformed for variance stabilization
284 using the DESeq2 function rlog (regularized-logarithm transformation). Batch effects were
285 removed using the function removeBatchEffect of the R package LIMMA (32). Gene with counts
286 lower than 5 in at least one sample were removed for downstream analyses. Differential expression
287 analysis was performed between control Th2 cells versus calcitriol stimulated Th2 cells using
288 DeSeq2. The design matrix was built to consider batch effects derived from the RNA isolation

289 process. DESeq2-independent filtering was applied (30) and P values were corrected for multiple
290 hypothesis testing by using the Benjamini-Hochberg (BH)-FDR adjustment (33).

291 The PPI network used in our network analysis was developed by Silverbush et al. (34). As
292 described in the original paper, this human PPI network was reconstructed by integrating large
293 scale PPI databases, drug response repositories, and cancer genomics data. Only the largest
294 connected component of the network was considered, resulting in an interactome of 15,500
295 proteins and 234,585 consensus-oriented interactions. Conversion between murine and human
296 gene IDs was performed using the BioMart conversion tool (35). We also assumed a one-to-one
297 correspondence between genes and their protein products in the entire analysis.

298 To identify the active signaling paths in control and calcitriol stimulated Th2 cells, we modelled
299 the transmission of the molecular signal as a sequential path on the PPI network (called a network
300 path) that starts from a receptor, connects the receptor to multiple intermediate proteins, and leads
301 to a transcription factor. Receptors and transcription factors were selected from a predefined list
302 based on their role in Th2 cell biology and IL-2 expression (**Figure 4-table supplement 1**). CD3,
303 CD28, IL-4R, IL-13R were selected based on their role in Th2 differentiation. The IL-2R complex
304 was included due to being a target of vitamin D signaling. TGFβRs were selected based on the
305 immunomodulatory activity of this signaling path in CD4+ T cells. role in mediating
306 immunoregulation. Using this subset of receptors and transcription factors as input for the
307 implementation of our network analysis, we computed all the shortest paths connecting each
308 receptor-transcription factor pair on the PPI network. For both control and calcitriol stimulated
309 Th2 cells, we ranked each network path based on the average expression of the path's nodes. The
310 top selected paths represent the most active downstream processes in Th2 cells in each condition.

311 ***mRNA isolation, reverse transcription, and real-time RT-PCR***

312 Total RNA from in vitro polarized Th2 cells was isolated with the RNeasy Mini Kit (Qiagen).
313 First-strand cDNA synthesis was performed with the Omniscript kit (Qiagen). Quantitative real-
314 time PCR was performed with the SsoFast EvaGreen Supermix Kit (BioRad) on a AriaMx Real-
315 time PCR System (Agilent) as per manufacturer's instructions. Primers sequences used in this
316 study are: Gsdma (sense: 5'-TGC TGT CAA AGG ACG CTA TG-3'; antisense: 5'-TCA ACC
317 AGC TTC AGT TGC AC-3'), IL-2 (sense: 5'-CCC ACT TCA AGC TCC ACT TC-3'; antisense:
318 5'-ATC CTG GGG AGT TTC AGG TT-3'), Ikfz3 (5'-TGT CAC CTC TGC AAC TAC GC-3'; 5'-
319 TTC CGC AGA ACT CAC ACT TG-3'), Ormdl3 (sense: 5'-CAC ACG GGT GAT GAA C AG
320 TC-3'; antisense: 5'-CTT TGC CTT GGT CTG GAG TC-3'), Stat3 (sense: 5'-GAG GAG CTG
321 CAG AAA GT-3'; antisense: 5'-TCG TGG TAA ACT GGA CAC CA-3'), Stat5a (sense: 5'-TAC
322 ATG GAC CAG GCT CCT TC-3'; antisense: 5'-GTC AAA CTC GCC ATC TTG GT-3'), Stat5b
323 (sense: 5'-TGT GGA TAC AGG CTC AGC AG-3'; antisense: 5'-TGG GTG GCC TTA ATG TTC
324 TC-3'). Relative gene expression levels were calculated with the $2^{-\Delta\Delta Ct}$ method, with normalization
325 to the murine ribosomal L32 as the housekeeping gene. Data are presented as fold induction over
326 the respective control groups (vehicle or WT). All standard procedures were performed according
327 to the manufacturer's instructions.

328 ***Quantification and statistical analysis***

329 For each figure the number of replicates per experiment is indicated in the corresponding figure
330 legend. In the figures, mean and standard error of the mean (s.e.m.) are presented and error bars
331 represent the mean ± s.e.m. Two group comparisons were analyzed using unpaired two-tailed
332 Student's t-tests (parametric data) and Mann–Whitney U-test (non-parametric data). Multiple
333 group comparisons were analyzed with Kruskal-Wallis and One-way ANOVA test with Tukey's
334 post hoc analysis. *In vivo* experiments were analyzed using Mixed-effect analysis or Two-way

335 ANOVA test with Holm-Šidák's post-hoc analysis (factors: genotype & exposure, diet &
336 exposure). Prism 9.2 (GraphPad Software) was used to calculate statistics. P values of less than
337 0.05 were considered statistically significant.

338

339 **RESULTS**

340 **Integrative bioinformatics identifies the potential control of key asthma and autoimmune**
341 **loci in 17q12-21.1 and 17q21.2 by vitamin D**

342 To address the genetic and molecular mechanisms by which vitamin D can influence asthma,
343 allergic and autoimmune disease risk, we studied the genetic loci of two chromosome regions of
344 interest: 1) the 17q12-21.1 region, that includes the well-known asthma-associated *ORMDL3* gene
345 (36), and 2) the 17q21.2 region, that includes the *STAT5* gene, known to be extensively associated
346 with autoimmune diseases (37,38). We first examined the entire set of significant disease and trait
347 associations in the Chr17q12-21.1 (181 associations) and Chr17q21.2 (100 associations) loci using
348 the NHGRI-EBI GWAS Catalog (24). Both regions had multiple Th1 and Th2 diseases
349 associations with at least one significant SNP. Chr17q12-21.1 had the highest number of
350 associations related to Th2 diseases (**Figure 1*A***) and 17q21.2 had the highest number of
351 associations related to Th1 diseases (**Figure 1-figure supplement 1*A***). To address the possible
352 link to vitamin D intake, we next investigated a potential overlap of these SNPs with VDR binding
353 sites. Out of the 169 VDR binding sites on Chr17, seven were in the 17q12-21.1 locus,
354 concentrated in two bands on or near *IKZF3* and *ZPBP2* (**Figure 1*B***). These VDR binding sites
355 also overlapped with RXRA binding sites (**Figure 1*B***). To assess their functional relevance, we
356 searched for expression quantitative trait loci (eQTLs) in these VDR binding regions. We found
357 that four cis-eQTLs control *IKZF3* expression in whole blood and EBV-transformed lymphocytes:

358 rs2941522 and rs12946510 in the enhancer region targeting *ORMDL3* and *IKZF3*, and rs1453559
359 and rs35564481 in the enhancer region targeting *ORMDL3*, *GSDMA* and *GSDMB* (**Figure 1*B***).
360 Rs1453559 and rs2941522 have previous GWAS associations with both asthma and autoimmune
361 diseases (39–41), rs12946510 has previous GWAS associations with autoimmune diseases
362 (42,43), and rs35564481 has no known GWAS associations. For the 17q21.2 locus, the only VDR
363 binding site resides near the gene *PSMC3IP* in an enhancer site targeting *STAT5A* (**Figure 1-figure**
364 **supplement 1*B***). PSMC3IP expression is controlled by three eQTLs overlapping with this VDR
365 binding site (rs4793244, rs62078362 and rs111708606), none of which have any known disease
366 associations. These results suggest that vitamin D binding is critical in this genomic region.

367 We next examined the linkage disequilibrium (LD) pattern between the Th1/Th2-associated SNPs
368 and the SNPs in the VDR binding sites (**Figure 1*C***). Out of the seven SNPs with VDR binding
369 sites identified in 17q12-21.1 and 17q21.2, the first four in 17q12-21.1 (rs2941522, rs12946510,
370 rs35564481, rs1453559) were in a high-LD block with many other Th1-Th2 associated SNPs in
371 the same region. These same four SNPs in 17q12-21.1 were also in high-LD with two SNPs in
372 *ZPBP2* and *ORMDL3* (rs12936231 and rs4065275, respectively) that were previously shown to be
373 functionally relevant to asthma (3,4,16). Additionally, two of the three SNPs with VDR binding
374 sites in 17q21.2 (rs4793244 and rs62078362) were in strong-LD with three other Th1-Th2
375 associated SNPs in the17q21.2 region (rs11871801, rs2006141, rs4793090). Overall, these results
376 highlight strong statistical association between vitamin D binding sites and multiple genotypic
377 variations linked to asthma, autoimmune and allergic diseases.

378 Two SNPs in *ZPBP2* and *ORMDL3* (rs12936231 and rs4065275, respectively) that were
379 previously shown to be functionally relevant to asthma (3,4,16), were also in high linkage
380 disequilibrium with the four SNPs that we identified in the VDR binding regions of the 17q12-

381 21.1 loci (**Figure 1*C***). Importantly, in both the 17q12-21.1 and 17q21.2 regions, the VDR binding
382 sites coincide with CTCF and IKZF3 binding sites, as well as H3K27ac peaks indicating active
383 enhancer sites (**Figure 1*B*, Figure 1-figure supplement 1*B***). In particular, the two enhancer sites
384 in 17q12-21.1 (GH17J039753 and GH17J039859) were both predicted to interact with the
385 *ORMDL3* promoter region (**Figure 1*B***), and the enhancer site in 17q21.2 (GH17J042576) was
386 predicted to interact with the *STAT5A* promoter region (**Figure 1-figure supplement 1*B***). This
387 suggests a similar mechanism to the one described in (4), whereby SNPs in LD with each other in
388 these enhancer sites affect VDR and CTCF binding, the co-dependence of which in turn could
389 modulate *ORMDL3* and *STAT5A* expression. Although it has been shown that CTCF binding sites
390 can be vitamin D-sensitive (7), no such sites were found in our genomic regions of interest (**Figure
391 1*B*, Figure 1-figure supplement 1*B***).

392 Next, we investigated cord blood gene expression data in the Vitamin D Antenatal Asthma
393 Reduction Trial (VDAART) (see Methods) and looked at the genes of interest in the 17q12 and
394 17q21 regions and their interaction with cord blood vitamin D levels as predictors of
395 asthma/wheeze risk at age 3 year of age. After adjusting for relevant covariates (see Methods), the
396 baseline expression term of *IKZF3* was not found to be significantly associated with asthma risk,
397 while the interaction between vitamin D and *IKZF3* was statistically significant (p-val. < 0.05),
398 suggesting that the association of *IKZF3* expression with asthma risk was mediated by vitamin D
399 levels in the cord blood (**Figure 1- table supplement 1; Figure 1-figure supplement 1*C***).

400 Based on our bioinformatic analysis of the Chr17q12 and 17q21 regions, we hypothesize that low
401 vitamin D tissue levels is associated with decreased *IKFZ3* expression and increased expression
402 of *ORMDL3*, *STAT3*, *STAT5A*, *STAT5B*, and *IL2*.

403 **Vitamin-D receptor (VDR) is expressed in Th2 cells in allergic airway inflammation**

404 To test our hypothesis of vitamin D activity at the Chr17q12-21 locus we utilized a mouse model
405 of allergic airway inflammation and identified vitamin D responsive leukocyte subsets in house
406 dust mite (HDM)-sensitized and challenged mice using flow cytometry (**Figure 2*A***, **Figure 2-**
407 **figure supplement 1*A-C***). VDR expression was significantly induced in HDM sensitized and
408 challenged mice and almost absent in leukocytes isolated from control (vehicle) lungs (**Figure 2-**
409 **figure supplement 2*C***). Within the CD45+ population, VDR expression was high in CD4+ T cells
410 ($p= 0.0357$), while only very few CD8+ T cells and CD19+ B cells expressed VDR (**Figure 2*B***,
411 **Figure 2-figure supplement 1*B* HDM**). Within the CD4+ T cell population, highest VDR
412 expression was detected in Gata3+ Th2 cells ($p= 0.002$ vs Tbet+ and $p< 0.0001$ vs Foxp3+ T cells).
413 VDR expression was very low in Tbet+ Th1 and CD4+ Foxp3+ Treg cells (**Figure 2-figure**
414 **supplement 1*C* HDM**). The differential expression of VDR in Th2 cells was further validated by
415 western blot analysis using naïve CD4+ T cells immediately after isolation (0hrs), after activation
416 with CD3/CD28 for 48 hrs and in *in vitro* polarized Th1, Th2 and iTreg cells with well-defined
417 culture conditions (**Figure 2-figure supplement 2*A***, see Methods section). VDR expression
418 appeared as early as day 1 of Th2 culture conditions and gradually increased during the
419 polarization process (**Figure 2-figure supplement 2*B***). In the absence of the VDR ligand vitamin
420 D, VDR expression localized to the cytoplasm of Th2 cells. Addition of the VDR ligand calcitriol
421 led to a strong translocation of VDR into the nucleus, suggesting functionality of the expressed
422 receptor in the presence of its ligand (**Figure 2-figure supplement 2*C***). These results identify Th2
423 cells as vitamin D targets in allergic airway inflammation.

424

425 **Vitamin D status regulates the expression of key genes on Chromosome17q12-21.1 and**
426 **Chr17q21.2**

427 Taking cell type specific gene expression and selective expression of VDR in Th2 cells into
428 account, we next analyzed the expression of genes encoded on Chr17q12-21.1 and 17q21.2 loci in
429 WT and vitamin D deficient Th2 cultures as well as in Th2 cells post calcitriol stimulation.

430 Vitamin D deficiency differentially regulated the expression levels of several Chr17q12-21.1
431 encoded genes, with lower expression of *Ikzf3*, *Ormdl3* and *Gsdma* (all p=0.0286) (**Figure 2*D***).
432 Conversely, stimulation with calcitriol induced the expression of the same genes (all p=0.043)
433 (**Figure 2F**). Expression of the Chr17q21.2 genes *Stat3*, *Stat5a* and *Stat5b* was not affected by
434 vitamin D deficiency (**Figure 2*E***). However, after calcitriol stimulation *Stat5a* (p=0.0082) and
435 *Stat5b* (p=0.003) genes were strongly suppressed and *Stat3* (p= 0.0048) expression was increased
436 in Th2 cells. (**Figure 2*G***). These results hint to a protective role of vitamin D in allergic airway
437 inflammation, by regulating the expression of the IL-2 downstream signaling molecules *Stat5a*
438 and *Stat5b*.

439

440 **Deficiency in vitamin D signaling augments allergic airway inflammation**

441 To decipher the protective role of vitamin D signaling in allergic airway inflammation, we
442 employed vitamin D deficient and $VDR^{-/-}$ mice (**Figure 3*A***) (28). HDM sensitization of vitamin
443 D deficient mice led to a stronger reaction to the allergen resulting in more prominent peri-
444 bronchial and perivascular leukocytic infiltrates (**Figure 3*B***). This phenotype was accompanied
445 by lower VDR expression in CD4+ T cells isolated from HDM-exposed lungs compared to WT
446 (**Figure 3*C***). Vitamin D deficiency led to a robust increase in total immunoglobulin (Ig)E levels
447 (**Figure 3*D***). Histological findings were associated with higher total BAL leukocyte (p= 0.0008)
448 (**Figure 3*E***), eosinophil (p= 0.0002) (**Figure 3*F***) and lymphocyte (p= 0.0023) (**Figure 3*G***)
449 numbers in vitamin D deficient mice, while neutrophil numbers were not affected **Figure 3-figure**

450 **supplement 1*A)***. Th2 cell numbers (p= 0.0127) were also higher in the HDM exposed mice
451 (**Figure 3*H***) in a manner that was independent of T helper cell skewing (**Figure 3-figure**
452 **supplement 1*B, C***). Differentiation and recruitment of Th17 and IL-10 producing CD4+ T cells
453 was not affected by vitamin D deficiency (**Figure 3-figure supplement 1*A, B***). To validate these
454 findings from vitamin D deficiency, we next employed $VDR^{-/-}$ mice (see Methods). As with the
455 vitamin D deficient mice, HDM sensitization and challenge of $VDR^{-/-}$ mice led to an increased Th2
456 immune response. The lung phenotype in the $VDR^{-/-}$ mice was marked by dense leukocytic
457 infiltrates around and mucus plugs in the airways (**Figure 3*B***). The augmented systemic and local
458 immune response increased total IgE titers (p= 0.0489), and total BAL (p< 0.0001 vs WT HDM
459 and p= 0.003 vs Vit D deficient HDM), eosinophil (p< 0.0001 vs WT HDM and Vit D deficient
460 HDM), total lymphocytes (p=0.0194 vs WT HDM and p= 0.0421vs Vit D deficient HDM) and
461 Th2 cells (p= 0.0009 vs WT HDM) (**Figure 3*D-H***). $VDR^{-/-}$ did not significantly affect recruitment
462 of neutrophils, Treg and Th17 cells (**Figure 3-figure supplement 1*A, B, C***).

463 To explore the mechanisms underlying the augmented Th2-phenotype in the lungs of vitamin D
464 deficient and $VDR^{-/-}$ mice after HDM allergen challenge, we analyzed the transcriptional profiles
465 of in vitro polarized Th2 cells from WT and vitamin D deficient mice (**Figure 3*I***). Differential
466 expression and enrichment analysis revealed dysregulation of several pathways implicated in Th2-
467 cell activation, cytokine production, proliferation, and survival with prominent changes in the IL-
468 2/ STAT5 - pathway in vitamin D deficient Th2 cells (p= 0.0014) (**Figure 3*J***, **Figure 3-table**
469 **supplements 1, 2**). The effects of impaired vitamin D signaling on these pathways was confirmed
470 by qRT-PCR and flow cytometry. Baseline expression of IL-2 was markedly increased at both the
471 RNA (p= 0.0286)) and protein levels (p= 0.0079) in vitamin D deficient and $VDR^{-/-}$ Th2 cells
472 (**Figure 3*K, L***). In Vitamin D deficient and $VDR^{-/-}$ Th2 cell *in vitro* incubation, the elevated IL-2

473 levels were accompanied by a sharp increase in IL-13 production (VitD deficient: $p < 0.0001$; $VDR^{-/-}$: $p = 0.0141$) (**Figure 3-figure supplement 2**).

475 Taken together, these results indicate a critical role for vitamin D/VDR signaling in regulating type
476 2 inflammation and identify the IL-2/ Stat5 pathway as a downstream target of vitamin D in Th2
477 cells.

478

479 **Vitamin D suppresses the activation of the IL-2/Stat5 pathway and cytokine production in**
480 **Th2 cells**

481 To ascertain the vitamin D dependent regulation of the IL-2/Stat5 pathway and the impact on the
482 effector program of Th2 cells, we first analyzed the transcriptional profile of WT Th2 cells exposed
483 to calcitriol during differentiation (**Figure 4*A***). Gene ontology enrichment analysis of biological
484 processes revealed regulation of several processes impacting inflammatory responses, including
485 chemotaxis and activation of cells (**Figure 4-table supplement 1**). Calcitriol stimulation of Th2
486 cells affected several immune related disease pathways, including asthma (**Figure 4-figure**
487 **supplement 1, Figure 4-table supplement 2**). Gene set enrichment analysis (GSEA), performed
488 on the differentially expressed genes, highlighted the negative regulation of IL-2/Stat5 pathway in
489 Th2 cells by calcitriol (**Figure 4*B***, **Figure 4-table supplement 3**). Calcitriol stimulation
490 suppressed the expression of *Il2* ($p<0.0001$), *Stat5a* ($p<0.0008$) and *Stat5b* ($p<0.0008$) genes
491 (**Figure 4*C***). Concordantly, levels of activated Itk (phospho-Itk) ($p = 0.029$) and expression of the
492 IL2Rβ (CD25) ($p = 0.0441$) were reduced on a per cell basis (**Figure 4*D***).

493

494 Next, the impact of calcitriol stimulation on the effector function of Th2 cells was assessed by
495 flow cytometric analysis for the T2 cytokine IL-13. Activation of the vitamin D/VDR pathway led
496 to significant suppression of IL-13 production in CD4+ T cells (p= 0.0012) (**Figure 4*E***).

497 To further delineate the molecular impact of vitamin D on Th2 cell biology, we integrated the
498 murine transcriptional profile with a recently developed human Protein-Protein Interaction (PPI)
499 database (34). By modeling the signal transduction process as a sequential path on the PPI network
500 that starts from a receptor and propagates downstream to a transcription factor via multiple
501 intermediate proteins (for details see Methods section, **Figure 4-figure supplement 2*A***), we
502 inferred the active signaling flow in Th2 cells for control (vehicle) and calcitriol stimulated Th2
503 cells. As input of our network analysis, we selected a subset of receptors and transcription factors
504 that are known to be involved in CD4+ T cell activation, Th2 cell differentiation, and cytokine
505 production (**Figure 4-table supplement 4**). For clarity of the figure, we display the gene names.
506 Corresponding protein names are attached in **Figure 4-table supplement 5**. In control Th2 cells,
507 our network analysis revealed the engagement of a variety of receptors including IL4R, IL2RA,
508 CD28, and TNF-receptors. Downstream to these receptors, the most active signaling paths
509 highlighted the activation of STAT3, STAT5A/B, NFkB1, and IKZF1 transcription factors
510 (**Figure 4-figure supplement 2*B***) via multiple adapter proteins of the TRAF and JAK family.
511 Interestingly, these transcription factors are known to be involved in differentiation and activation
512 pathways in Th2 cells Conversely, after calcitriol stimulation, signal from IL4R, CD28 and
513 TNFSF8 propagated over different interaction partners (**Figure 4*F***). Calcitriol specific edges are
514 highlighted in orange color. Molecular mediators included the cytoskeletal proteins VAV1 and
515 RACK1 and emphasized activation of the transcription factors AP-1 (FOS/JUND dimer) and
516 NFATC1.

517

518 Our network analysis highlighted a central role of the transcriptional repressor IKZF1 (IKAROS)
519 upon calcitriol stimulation, which was targeted by multiple downstream mediators including
520 IKZF3 (AIOLOS). Notably, the IKZF3 gene encodes for the AIOLOS protein, a direct interaction
521 partner of the IKZF1-encoded IKAROS. Both transcription factors, as homo- and heterodimers,
522 suppress IL-2 expression on the transcriptional levels in mouse and human lymphocytes (44).
523 Calcitriol increased the number of edges connecting intermediate proteins to the transcriptional
524 repressor IKAROS. Among the connecting proteins, AIOLOS interaction with IKAROS was
525 implicated in repression of IL-2 expression in Th2 cells by vitamin D.

526 Absence of STAT5A/B mediators in the active signaling paths of calcitriol stimulated Th2 cells
527 further suggested repression of the Th2 cell STAT5 pathway with calcitriol compared to control
528 (**Figure 4-figure supplement 2*B***). To ensure that the above findings were not restricted to the
529 C57BL/6 mouse strain, the inverse experiment was performed in Balb/c mice. This mouse strain
530 is commonly used for type 2 driven inflammation.

531

532 Taken together, these results indicate that the specific suppression of the IL-2/Stat5 pathway by
533 vitamin D results in reduced cytokine production by Th2 cells. Our findings suggest that this
534 suppression was mediated by the vitamin D dependent regulation of IKAROS (IKZF1) through
535 the induction of AIOLOS (IKZF3).

536

537 **Vitamin D supplementation alleviates the allergic phenotype in the lung by suppressing type**
538 **2 cytokine production in a dose dependent manner**

539 To test if vitamin D supplementation prevents the development of T2 driven allergic inflammation
540 in the lung, custom rodent diets with select vitamin D doses were used: 400 IU/kg chow (400 IU;
541 low), 1000 IU/kg chow (1000 IU; regular) and 4000 IU/kg chow (4000 IU; high) (**Figure 5- figure**
542 **supplement 1*A*,** see Methods section). The 1000 IU group was used as the control group, as it
543 contains the average amount of vitamin D fortified in standard rodent chow. HDM exposure led
544 to recruitment of leukocytes into the lung tissue and BAL (**Figure 5*A, B;* Figure 5- figure**
545 **supplement 1*B***), with a predominant eosinophilic and lymphocytic infiltrate as well as high
546 numbers of IL-13+ Th2 cells (**Figure 5*C-E***). There were trends for higher cellular infiltration in
547 the airways when mice were supplemented with the low vitamin D doses (400 IU), but these
548 inflammatory responses were not significantly different from the phenotype observed with 1000
549 IU. Lung and airway pathology were similar between these dosing groups, with similar numbers
550 and frequencies of the different leukocyte populations. In sharp contrast, dietary supplementation
551 with the higher vitamin D dose (4000 IU) decreased the inflammatory phenotype in HDM exposed
552 mice compared to the 400 IU and 1000 IU dosed animals. Concordant with the histological
553 findings, BAL leukocytes ($p< 0.0001$) were decreased with marked reductions in BAL eosinophil
554 ($p=0.0016$), lymphocyte ($p=0.026$) and neutrophils numbers ($p=0.0005$) (**Figure 5*B, D;* Figure 5-**
555 **figure supplement 1*C***), and the frequency of IL-13+ Th2 cells was significantly reduced in the
556 lungs with 4000 IU of vitamin D ($p= 0.0066$ vs 400 IU HDM; $p=0.0011$ vs 1000 IU HDM) (**Figure**
557 **5*E***). Of note, dietary supplementation with high vitamin D levels, increased VDR expression in
558 CD4+ T cells from HDM exposed lungs ($p< 0.0001$) (**Figure 5- figure supplement 1*C***).

559 To ascertain that dietary supplementation with vitamin D specifically altered mouse Th2 cell
560 differentiation and the effector program, splenic naïve CD4+ T cells from 400 IU and 4000 IU
561 mice were studied. Of interest, naïve CD4+ T cells did not express VDR until they were exposed

562 to Th2 polarizing conditions. Gata3 expression on per cell basis was lower in 4000 IU Th2 cells
563 (p= 0.0286) (**Figure 5- figure supplement 2*A***). This was accompanied by higher VDR protein
564 expression (p= 0.0286) (**Figure 5- figure supplement 2*B***). The expression of IL-2 (p= 0.0004)
565 and the Th2 cytokines IL-13 (p= 0.0159) and IL-5 (p= 0.0159) were lower in 4000 IU Th2 cultures
566 (**Figure 5- figure supplement 2*C-E***).

567 To explore the specific induction of Aiolos expression for vitamin D mediated suppression of IL-
568 2 production in Th2 cells, Aiolos expression was monitored throughout Th2 differentiation. Aiolos
569 expression gradually increased under Th2 polarizing conditions in CD4+ T cells, starting as early
570 as day 1 of in vitro culture (**Figure 5*F***). Simultaneous exposure to calcitriol further increased
571 Aiolos protein levels compared to vehicle in Th2 cells (p= 0.0079) (**Figure 5*G***).

572 To test if vitamin D exerts its inhibitory effect on IL-2 production via Aiolos induction, Ikzf3$^{-/-}$
573 mice were employed, exposed to Th2 polarizing conditions and assessed for IL-2 production after
574 calcitriol exposure. IL-2 production in control Ikzf3$^{-/-}$ Th2 cultures was significantly higher
575 compared to WT Th2 cells. Calcitriol significantly reduced IL-2 levels in both, WT (p= 0.0001)
576 and Ikzf3$^{-/-}$ Th2 cells (p= 0.0001) (**Figure 5*H***); however, the suppressive effect of calcitriol on IL-
577 2 production was significantly higher in WT Th2 cells (~ 65% inhibition) compared to Ikzf3$^{-/-}$ Th2
578 cells (~40% inhibition) (p= 0.0001) (**Figure 5*H***).

579 Taken together, these results indicated that vitamin D can regulate Aiolos expression and
580 suggested a role for Aiolos as a downstream effector for selectively fine-tuning Th2 cell IL-2
581 production by vitamin D.

582

583 **DISCUSSION**

584 We utilized human genetics to identify SNPs on chromosome 17q12-21.1 and 17q21.2 that were
585 within GWAS regions for Th1 and Th2 autoimmune diseases. Of note, many of these SNPs were
586 within VDR binding sites. We then determined by eQTL analysis of the genes in these two
587 genomic regions that IKZF3 expression was controlled by four cis-eQTLs in the enhancer region
588 targeting ORMDL3 and IKZF3, and in the enhancer region targeting ORMDL3, GSDMA and
589 GSDMB. Next, we demonstrated that two SNPs in CTCF binding sites were in strong LD with
590 these 4 eQTL SNPs and that the two enhancer sites in 17q12-21.1 were both predicted to interact
591 with the ORMDL3 promoter region, and the enhancer site in 17q21.2 was predicted to interact
592 with the STAT5A promoter region thus, suggesting a plausible human molecular genetic
593 mechanism by which vitamin D could activate IKZF3 to repress ORMDL3 and immune system
594 development. Finally, we leveraged bulk RNAseq in the cord blood of the VDAART trial to show
595 that an interaction for vitamin D level and IKZF3 expression that was associated with reduced
596 asthma risk at 3 years of age. **Figure 5- figure supplement 3** depicts the influence of vitamin D
597 binding sites on the genes in the 17q12-21 region.

598 To confirm our human molecular genetic findings, we chose to utilize mouse models of allergic
599 lung inflammation. We show strong VDR expression in CD4+ Th2 cells and alterations in
600 chr17q12-21.1 and 17q21.2 gene expression induced by vitamin D status. Expression of VDR has
601 been reported for airway epithelial cells and different immune cell types present in the lung (45).
602 In lymphocytes, *ex vivo* and *in vitro* studies describe low baseline VDR transcript expression levels
603 that were transiently increased by activating signals and calcitriol stimulation (46). Here, we report
604 a differential VDR expression pattern in CD4+ T cell subsets from allergic inflamed lungs and
605 post lineage specific cytokine stimulation *in vitro*, with strongest expression in Th2 cells.
606 Activation of VDR suppressed IL-2, IL-5, and IL-13 production by Th2 cells. The expression of

607 VDR in Gata3+Th2 cells in the lung might represent an endogenous control mechanism to curb
608 the pathogenic cell activity and cytokine production after repetitive allergen contact. *Ex vivo* and
609 *in vitro* Th1, nTreg and iTreg cells expressed low VDR protein levels at baseline. It remains to be
610 determined whether other Th-subsets described in allergic inflammation express VDR at baseline
611 and if either calcitriol or other secondary signals, specific for each subset, could induce VDR
612 expression during inflammation.

613 Vitamin D deficiency that had been introduced over two generations, impaired vitamin D
614 signaling and led to an augmented allergic phenotype in the lung after allergen exposure with a
615 dominating Th2-signature locally and systemically. This was likely due to specific deregulation of
616 Th2 cells instead of Th cell skewing, since neither Th17 nor Treg development and recruitment
617 were significantly affected. In contrast, in mice supplemented with high vitamin D doses over two
618 generations, VDR expression and consequently vitamin D responsiveness was higher in CD4+ T
619 cells from the animals' lungs, almost completely abrogating the inflammatory process in the lung
620 after allergen challenge. While the vitamin D dose in the mice was chosen to replicate the
621 VDAART trial dose in the mouse model, the duration of supplementation was adapted to the
622 protocol for generating vitamin D deficient mice. Both factors might influence the outcome here
623 compared to prior rodent studies with inconclusive results. We provide a discussion of vitamin D
624 toxicity in our response to the reviewers. More work to determine the exact levels of vitamin D
625 that confer this protective effect in the mice would also be worthy of further investigation.

626

627 Differentiation of Th2 cells is driven by IL-4 induced Gata3 expression in naïve CD4+ T cells.
628 This process depends on a positive feedforward loop by IL-2 and its downstream STAT5 signaling
629 pathway for the effective expression of IL-4 (47). Therefore, either interfering with Gata3

630 expression or with the IL-2 pathway represents a promising strategy to finetune Th2-driven
631 immunity. Our data highlight the specific regulation of the IL-2/STAT5 pathway by vitamin D.
632 Vitamin D deficiency and impaired VDR signaling caused elevated IL-2 production by Th2 cells,
633 leading to high IL-13 production. Elevated IL-13 levels *in vivo*, could amplify the local T2
634 responses in the lung. In sharp contrast, exposure of polarizing Th2 cells to calcitriol was able to
635 suppress IL-2 production, reduce expression and activation of STAT5A/B and therefore reduce
636 IL-13 production by Th2 cells. The transcription factor AIOLOS has previously been shown to
637 suppress IL-2 expression at the transcriptional level (44). We report here a vitamin D mediated
638 induction of Aiolos expression in Th2 cells, that is impaired by vitamin D deficiency. High Aiolos
639 expression coincided with lower IL-2 production, ameliorated STAT5A/B expression, and reduced
640 IL-13 production in Th2 cells. *In vitro* Th2 polarization of naïve CD4+ T cells isolated from mice
641 supplemented with higher vitamin D levels, without further exogenous calcitriol stimulation,
642 developed a weakened Th2 phenotype, characterized by lower IL-2, IL-5, and IL-13 production.
643 Since naïve CD4+ T cells do not express VDR, these results, together with our human data,
644 implicate changes in chromosomal accessibility by high vitamin D in the developing immune
645 system, which needs further investigation.
646 Experiments here with Ikzf3$^{-/-}$ mice demonstrated significant reductions in vitamin D mediated
647 control of Th2 cell cytokine production, but the vitamin D response was not completely
648 impaired, suggesting additional mechanisms for vitamin D regulation of Th2 cells – several
649 possibilities were uncovered by our PPI analyses. These will be the subject of future research. In
650 addition, we only investigated a Th2 mouse model of asthma and have not extended our mouse
651 work to Th1 models of autoimmunity. We acknowledge that the impact of vitamin D on Th2
652 biology is conflicting in the literature. While several groups report Th2 promoting activity, we,

653 and others, show inhibition of type 2 cytokine production (48–51). These discrepancies could be
654 due to the model system studied, e.g., PBMC and purified CD4+ T cells, or the dose of vitamin
655 D or the mouse strain.

656 We have still to consider other asthma genes that might be linked to these two genetic loci as there
657 are likely other VDR binding sites of importance in both asthma and Th1 autoimmunity. Our
658 preliminary results confirm that three asthma susceptibility loci: 2q12.1 (IL1RL1), 6p21.32 (HLA-
659 DQA1/B1/A2/B2) and 22q12.3 (IL2RB) each have VDR and IKZF3 binding sites either in
660 enhancers predicted by GeneHancer to target these genes or within these genes themselves. It is
661 important to consider other data that might have enhanced the results that we present here. For our
662 human genetic data, additional use of ChIP or co-IP to establish STAT induction and activation
663 would have been of potential value. For our mouse studies, additional cytokine measurements in
664 the mice as well as measurement of airway resistance would have added to the pathophysiological
665 data linking IKFZ3 expression to TH2 response. Finally, quantification of histology and confocal
666 images could provide an overview of VDR expression in the lungs.

667

668 In summary, we have leveraged clinical trial data, molecular genetic bioinformatic data and mouse
669 model data to outline for the first time, a comprehensive molecular genetic mechanism for how
670 vitamin D influences not only asthma development, but both Th1 and Th2 autoimmune disease.
671 The significance of these findings relates to the high prevalence of vitamin D deficiency, especially
672 during pregnancy, and the strong possibility that the epidemic of asthma and autoimmunity might
673 be significantly reduced if serum vitamin D levels were elevated worldwide.

674

675 **List of Supplementary Materials**

676 Fig S1 to S11

677 Tables S1 to S9

678

679 **Acknowledgments:** We wish to thank the VDAART trial participants and clinical staff for their
680 critical work on the VDAART study. We wish to thank also our Channing colleagues for
681 their comments.

682 **Funding:**

683 National Heart, Lung, and Blood Institute grant 5P01HL132825
684 National Heart, Lung, and Blood Institute grant 5UH3OD023268
685 National Heart, Lung, and Blood Institute grant 5K25HL150336
686 German Society for Clinical Chemistry and Laboratory Medicine (DGKL) and the
687 German Research Foundation (DFG) grant KI 1868/3-1

688 **Author contributions:**

689 A.K. and S.T.W. jointly supervised this work. A.K., A.H. and S.T.W. designed the experiments,
690 analyzed data and wrote the manuscript. A.K., M.G.D., T.R.B., J.R.Q., A.O.S, J.K., T.N., H.Y.P.,
691 N.K. and R.E.A performed experiments. A.H., E.M., M.D.M. and R. C. analyzed data. M.D. and
692 K.G. provided critical mouse lines and scientific input. A.A.L. assisted on VDAART related
693 analyses. H.R. and B.D.L. supervised experiments and provided critical scientific input. All
694 authors critically reviewed the manuscript.

695 **Competing interests:** Dr. Weiss receives royalties from UpToDate and is an investor in Histolix.
696 All other authors declare that they have no competing interests.

697 **Data and materials availability:** All data are available in the main text or the supplementary
698 materials.

699

700 **Figure legends**

701 **Figure 1. VDR binding sites on Chr17q12 and q21.1 overlap with open chromatin signatures.**
702 ***A***, Significant disease and trait associations in 17q12-21.1 (y-axis), retrieved from the NHGRI EBI
703 GWAS Catalog, with at least one significant SNP (x-axis) in Chr17q12-21.1. Colored bars denote
704 autoimmune diseases mapped to Th1 (red bars) or Th2 (blue bars) driven immunity. ***B***, University
705 of California Santa Cruz (UCSC) Genome Browser tracks showing chromosomal location,
706 common dbSNPs, VDR-, RXR-, CTCF- and IKZF3-binding sites and H3K27Ac marks present in
707 the Chr17q12-21.1 locus. VDR binding sites overlapping with active regulatory elements are
708 highlighted by colored boxes. ***C***, Linkage disequilibrium (LD) between the significant SNPs in the
709 Chr17q12-21.1 (magenta) and 21.2 (green) region, highlighting Th1/Th2 associated SNPs (red and
710 blue, respectively), eQTLs in the VDR binding regions in Chr17q12 21.1 and 21.2 (yellow), and
711 functional asthma SNPs from the literature (cyan).

712

713 **Figure 1-figure supplement 1. *A*,** Significant disease and trait associations in 17q21.2 (y-axis),
714 retrieved from the NHGRI-EBI GWAS Catalog, with at least one significant SNPs (x-axis) in
715 Chr17q21.2. Colored bars denote autoimmune diseases mapped to Th1 (red bars) or Th2 (blue
716 bars) driven immunity. ***B*,** University of California Santa Cruz (UCSC) Genome Browser tracks
717 showing chromosomal location, common dbSNPs, VDR-, RXR-, CTCF- and IKZF3-binding sites
718 and H3K27Ac marks present in the Ch17q21.2 locus. VDR binding sites overlapping with active

719 regulatory elements are highlighted by colored boxes. ***C,*** Overview of the analyses conducted on
720 the VDAART transcriptomic and clinical data.

721

722 **Figure 2. VDR expression is elevated in Th2 cells and vitamin D regulated expression of genes**
723 **on Chr1q12 and Chr17q21.** ***A,*** Scheme of the house dust mite (HDM) induced airway
724 inflammation protocol. ***B,*** Flow cytometric analysis and cell frequencies of VDR expression in
725 CD45+ CD4+ T cells in the respective groups (n=4-5). ***C,*** Flow cytometric analyses and cell
726 frequencies of VDR expression in Th1 (Tbet+), Th2 (Gata3+) and Treg (Foxp3+) cells in the
727 respective groups (n=4-7). Quantitative RT-PCR analysis of relative mRNA expression levels of
728 genes encoded on Chr17q12-21.1 in (***D***) Th2 cultures of WT and vitamin D deficient mice and (***E***)
729 control and calcitriol stimulated cultures. Quantitative RT-PCR analysis of relative mRNA
730 expression levels of genes encoded on Chr17q21.2 in (***F***) Th2 cultures of WT and vitamin D
731 deficient mice and (***G***) control and calcitriol stimulated cultures. Gene expression levels were
732 normalized to the house keeping gene L32 and are expressed relative to the expression level in
733 WT (***D, F***) or WT-vehicle (***E, G***) Th2 cells. ($n \geq 4$ per group). Each symbol represents one mouse.
734 Numbers in flow plots indicate percentages. Error bars indicate the s.e.m. Statistical tests: two-
735 tailed Mann-Whitney U test (***B, C***). *$P < 0.05$, **$P < 0.01$, ***$P < 0.001$. Data summarize results
736 from two independent experiments.

737

738 **Figure 2-figure supplement 1. Baseline VDR expression is confined to the CD4+ Foxp3- Teff**
739 **cell population.** ***A,*** Gating strategy for the analysis of VDR expression in different leukocyte
740 populations in the lung. ***B,*** Flow cytometric analysis and cell frequencies of VDR expression in
741 CD45+, CD4+, CD8+ and CD19+ in the respective groups (n=4-5). ***C,*** Representative flow plots

742 of lung CD45+ CD4+ T cells isolated from saline and HDM- immunized and -challenged mice for
743 the co-expression of Foxp3 and VDR. Each symbol represents one mouse. Numbers in flow plots
744 indicate percentages. Error bars indicate the s.e.m. Statistical tests: two-tailed Mann-Whitney U
745 test. *P < 0.05. Data summarize results from two independent experiments.

746

747 **Figure 2-figure supplement 2. VDR expression is induced during CD4+ Th2 cell**
748 **differentiation**. ***A,*** Representative immunoblot for VDR expression in freshly isolated (0 hrs) and
749 activated CD4+ CD62L+ CD44- naïve T cells (48 hrs.) and in vitro polarized Th1, Th2 and iTreg
750 cells. Kidney samples of WT and VDR-/- mice were used as controls. ***B*****,** Representative
751 immunoblot for VDR expression in polarizing Th2 at the indicated days of in vitro culture. ***C*****,**
752 Representative image of VDR localization in in vitro polarized Th2 cells stimulated with vehicle
753 (EtOH, [% v/v]) or calcitriol.

754

755 **Figure 3. Vitamin D deficiency augments allergic airway inflammation.** ***A,*** Schematic
756 presentation of the different mouse strains used. ***B,*** Representative H&E-stained lung sections
757 from saline and HDM-exposed wild type (C57/BL6; WT), vitamin D deficient and VDR-/- mice
758 (x 10 magnification). Black arrows point to the peri bronchial infiltrate. ***C,*** Representative flow
759 plots assessing VDR expression in lung CD4+ T cells from the indicated groups. ***D,*** Total IgE
760 levels detected in the sera of respective groups. ***E-G,*** Absolute numbers of (***E***) leukocytes, (***F***)
761 eosinophils, and (***G***) lymphocytes in the airways of the respective groups. ***H,*** Frequencies of IL-
762 13 producing Th2 in the lung. Data summarize results from two or three independent experiments
763 with n>8 per group. ***I,*** Heat map showing differentially expressed genes between WT and vitamin

764 D deficient Th2 cultures identified by RNA-Sequencing analysis. Analysis and visualization were
765 performed with DESeq2. ***J,*** Overrepresentation analysis of Hallmark gene sets in the differentially
766 expression gene set. The x-axis represents the gene ratio in the respective gene set. Dot sizes denote
767 the number of genes in the respective pathway. The dot color indicates the FDR-adjusted p-value.
768 Analysis and visualization were performed with the clusterProfiler package. ***K,*** Quantitative RT-
769 PCR analysis of Il-2 mRNA expression in Th2 cultures from the respective groups (n=4 per group).
770 Gene expression levels were normalized to the house keeping gene L32 and are expressed as fold-
771 induction compared to WT Th2 cells. ***L***, Flow cytometric analysis and cell frequencies of IL-2
772 production in WT and VDR-/- Th2 cultures (n=5 per group). Each symbol represents one mouse.
773 Error bars indicate the s.e.m. Statistical significance was determined with: Mixed-effect analysis
774 with Holm-Šidák's post-hoc analysis (***D –H***), two-tailed Mann-Whitney U test (***K, L***). *P < 0.05,
775 **P < 0.01, ***P < 0.001, ****P < 0.0001. Data summarize results from two or three independent
776 experiments with n>8 per group.

777

778 **Figure 3-figure supplement 1. Vitamin D deficiency does not alter CD4+ IL-10 and IL-17A**
779 **expression allergic airway inflammation.** Frequencies of BAL neutrophils **(*A*)**, IL-10 (***B***) and
780 IL-17A (***C***) CD4+ T cells. Each symbol represents one mouse. Error bars indicate the s.e.m. Data
781 summarize results from two or three independent experiments with n>8 per group.

782

783 **Figure 3-figure supplement 2. Vitamin D deficiency increases IL-13 expression in Th2 cells.**
784 Flow cytometric analysis and frequencies of IL-13 expression in WT, vitamin D deficient and
785 VDR-/- Th2 cultures (n=5-9 per group). Each symbol represents one individual sample and data
786 summarize the results from two or three independent experiments. Error bars indicate the s.e.m.

787 Statistical tests: Kruskal- Wallis Test with Dunn's post-hoc analysis. *P < 0.05, **P < 0.01, ****P
788 < 0.0001.

789

790 **Figure 4. Vitamin D stimulation of polarizing Th2 cells suppresses the IL-2/Stat5 pathway.**
791 ***A,*** Heat map of differentially expressed genes between vehicle (EtOH [% v/v]) and calcitriol
792 treated WT Th2 cells. Analysis and visualization were performed with DESeq2. ***B***, Gene set
793 enrichment analysis (GSEA) of differentially expressed genes. Analysis and visualization were
794 performed with the clusterProfiler package. ***C***, Quantitative RT-PCR for Il-2, Stat5a and Stat5b
795 mRNA expression in Th2 cells exposed to either vehicle or calcitriol. Gene expression levels were
796 normalized to the house keeping gene L32 and are expressed as fold-induction compared to control
797 cells. ***D***, Flow cytometric analysis and mean fluorescence intensities of Itk and Il2rβ expression in
798 indicated groups. ***E***, Flow cytometric analysis and quantification of IL-13 expression in respective
799 groups. ***F***, Network analysis to visualize vitamin D induced molecular changes in the molecular
800 interactome of calcitriol stimulated CD4+ Th2. Predefined set of cell membrane receptors were
801 set as starting points (orange nodes) and annotated transcription factors were set as ending points
802 (blue). All intermediate proteins on the PPI are visualized as grey nodes. Molecular interactions
803 only overrepresented in calcitriol stimulated cells are shown as orange arrows. Each symbol in the
804 bar graphs represents one individual sample and data summarize the results from two or three
805 independent experiments with n≥ 5. Error bars indicate the s.e.m. Statistical test: two-tailed

806 Student's t-test (***C, E***) and two-tailed Mann-Whitney U-test (D). *P < 0.05, **P < 0.01, ***P <
807 0.001.

808

809 **Figure 4-figure supplement 1. KEGG pathways analysis post vitamin D stimulation.** List of
810 KEGG pathways enriched (p-adj. < 0.05) in DE genes after calcitriol stimulation. The x-axis
811 indicates the number of genes annotated to each pathway. The bar colors indicate the FDR-adjusted
812 p-value based on the colormap on the right side of the figure. The R package clusterProfiler was
813 used for the enrichment analysis and visualization.

814

815 **Figure 4-figure supplement 2. Active signaling pathways in Th2 cells.** ***A,*** Schematic
816 representation of the network analysis employed. ***B***, Network analysis to visualize active signaling
817 paths in control stimulated Th2 cultures. Predefined set of cell membrane receptors were set as
818 starting points (orange nodes) and annotated transcription factors were set as ending points (blue).
819 All intermediate proteins on the PPI are visualized as grey nodes. Molecular interactions only
820 overrepresented in control stimulated cells are shown as purple arrows.

821

822 **Figure 5. Prenatal vitamin D supplementation protects from asthma development.** ***A*****,** H&E
823 staining of representative lung sections of indicated experimental groups. Arrowheads point to peri
824 bronchial infiltrates. ***B-E*****,** Absolute numbers of total BAL (***B***) leukocytes, (***C***) eosinophils, (***D***)
825 lymphocytes, and (***E***) lung IL-13+ Th2 cells. ***F,*** Flow cytometric analysis of Aiolos expression in
826 differentiating Th2 cells at indicated time points. ***G***, QRT-PCR analysis of Ikzf3 transcripts in
827 respective groups. Expression levels were normalized to the house keeping gene L32 and are

828 expressed as fold change expression over the control samples WT-vehicle/ WT. ***H***, Flow
829 cytometric analysis of Aiolos expression in control and calcitriol stimulated Th2 cells. ***I,*** Flow
830 cytometric analysis and frequencies of IL-2+ cells in WT and Ikzf3-/- cultures post indicated
831 treatment. Each symbol represents and independent sample (n= 9 per group). Flow cytometric
832 analysis and quantification of VDR expression in lung CD4+ T cells of the respective groups. Each
833 symbol represents one individual mouse and data summarize the results from two to three
834 independent experiments with n>8 per group. Error bars indicate the s.e.m. Statistical significance
835 was determined with Mixed-effect analysis with Holm-Šidák's post-hoc analysis (***B-E***), two-tailed
836 Mann-Whitney U-test (***G, H***) and One-way ANOVA with Holm-Šidák's post-hoc analysis (***G***). *P
837 < 0.05, **P < 0.01, ***P < 0.001, ****P < 0.0001.

838

839 **Figure 5-figure supplement 1. Prenatal vitamin D supplementation increases VDR**
840 **expression in CD4+ T cells.** ***A***, Schematic presentation of the dietary intervention protocol and
841 breeding scheme with vitamin D. ***B,*** **Absolute neutrophil numbers in BAL.** ***C***, Flow cytometric
842 analysis and quantification of VDR expression in lung CD4+ T cells of the respective groups. Each
843 symbol represents one individual mouse and data summarize the results from two to three
844 independent experiments with n>8 per group. Error bars indicate the s.e.m. Statistical significance
845 was determined with One-way ANOVA with Holm-Šidák's post-hoc analysis. *P < 0.05, **P <
846 0.01, ***P < 0.001, ****P < 0.0001.

847

848 **Figure 5-figure supplement 2. Prenatal vitamin D supplementation mitigates Th2**
849 **development and cytokine production in vitro.** ***A-E***, Representative flow plots and cell
850 frequencies of (***A***) Gata3, (***B***) VDR, (***C***), IL-2, (***D***) IL-13, (***E***) IL-5 expression in indicated groups.

851 Each symbol represents one individual sample and data summarize the results from two to three
852 independent experiments (n= 4-10 per group). Error bars indicate the s.e.m. Statistical test: two-
853 tailed Mann-Whitney U-test (**a – e**). *P < 0.05, **P < 0.01, ***P < 0.001.

854 **Figure 5-figure supplement 3. Schematic summary of vitamin D molecular genetics in the**
855 **17q12-21 region.**

856

857 1. Litonjua AA, Weiss ST. Is vitamin D deficiency to blame for the asthma epidemic? J
858 Allergy Clin Immunol [Internet]. 2007 Nov [cited 2023 Sep 25];120(5):1031–5. Available
859 from: https://pubmed.ncbi.nlm.nih.gov/17919705/

860 2. Bouzigon E, Corda E, Aschard H, Dizier M-H, Boland A, Bousquet J, et al. Effect of
861 17q21 variants and smoking exposure in early-onset asthma. N Engl J Med [Internet].
862 2008 Nov 6 [cited 2023 Sep 25];359(19):1985–94. Available from:
863 https://pubmed.ncbi.nlm.nih.gov/18923164/

864 3. Kelly RS, Chawes BL, Guo F, Zhang L, Blighe K, Litonjua AA, et al. The role of the
865 17q21 genotype in the prevention of early childhood asthma and recurrent wheeze by
866 vitamin D. Eur Respir J [Internet]. 2019 Oct 1 [cited 2022 Dec 8];54(4). Available from:
867 https://pubmed.ncbi.nlm.nih.gov/31439681/

868 4. Schmiedel BJ, Seumois G, Samaniego-Castruita D, Cayford J, Schulten V, Chavez L, et
869 al. 17q21 asthma-risk variants switch CTCF binding and regulate IL-2 production by T
870 cells. Nat Commun [Internet]. 2016 Nov 16 [cited 2022 Dec 8];7. Available from:
871 https://pubmed.ncbi.nlm.nih.gov/27848966/

872 5. Raby BA, Lazarus R, Silverman EK, Lake S, Lange C, Wjst M, et al. Association of

873 vitamin D receptor gene polymorphisms with childhood and adult asthma. Am J Respir
874 Crit Care Med [Internet]. 2004 Nov 15 [cited 2023 Sep 25];170(10):1057–65. Available
875 from: https://pubmed.ncbi.nlm.nih.gov/15282200/

876 6. Camargo CA, Rifas-Shiman SL, Litonjua AA, Rich-Edwards JW, Weiss ST, Gold DR, et
877 al. Maternal intake of vitamin D during pregnancy and risk of recurrent wheeze in
878 children at 3 y of age. Am J Clin Nutr [Internet]. 2007 Mar 1 [cited 2023 Sep
879 25];85(3):788–95. Available from: https://pubmed.ncbi.nlm.nih.gov/17344501/

880 7. Devereux G, Litonjua AA, Turner SW, Craig LCA, McNeill G, Martindale S, et al.
881 Maternal vitamin D intake during pregnancy and early childhood wheezing. Am J Clin
882 Nutr [Internet]. 2007 Mar 1 [cited 2023 Sep 25];85(3):853–9. Available from:
883 https://pubmed.ncbi.nlm.nih.gov/17344509/

884 8. van der Pligt P, Willcox J, Szymlek-Gay EA, Murray E, Worsley A, Daly RM.
885 Associations of Maternal Vitamin D Deficiency with Pregnancy and Neonatal
886 Complications in Developing Countries: A Systematic Review. Nutrients [Internet]. 2018
887 May 18 [cited 2023 Sep 25];10(5). Available from:
888 https://pubmed.ncbi.nlm.nih.gov/29783717/

889 9. Roth DE, Abrams SA, Aloia J, Bergeron G, Bourassa MW, Brown KH, et al. Global
890 prevalence and disease burden of vitamin D deficiency: a roadmap for action in low- and
891 middle-income countries. Ann N Y Acad Sci [Internet]. 2018 Oct 1 [cited 2023 Sep
892 25];1430(1):44–79. Available from: https://pubmed.ncbi.nlm.nih.gov/30225965/

893 10. Cashman KD. Vitamin D Deficiency: Defining, Prevalence, Causes, and Strategies of
894 Addressing. Calcif Tissue Int [Internet]. 2020 Jan 1 [cited 2023 Sep 25];106(1):14–29.

895 Available from: https://pubmed.ncbi.nlm.nih.gov/31069443/

896 11. Litonjua AA, Lange NE, Carey VJ, Brown S, Laranjo N, Harshfield BJ, et al. The Vitamin
897 D Antenatal Asthma Reduction Trial (VDAART): rationale, design, and methods of a
898 randomized, controlled trial of vitamin D supplementation in pregnancy for the primary
899 prevention of asthma and allergies in children. Contemp Clin Trials [Internet]. 2014 [cited
900 2023 Sep 25];38(1):37–50. Available from: https://pubmed.ncbi.nlm.nih.gov/24614387/

901 12. Litonjua AA, Carey VJ, Laranjo N, Harshfield BJ, McElrath TF, O'Connor GT, et al.
902 Effect of Prenatal Supplementation With Vitamin D on Asthma or Recurrent Wheezing in
903 Offspring by Age 3 Years: The VDAART Randomized Clinical Trial. JAMA [Internet].
904 2016 Jan 26 [cited 2023 Sep 25];315(4):362–70. Available from:
905 https://pubmed.ncbi.nlm.nih.gov/26813209/

906 13. Litonjua AA, Carey VJ, Laranjo N, Stubbs BJ, Mirzakhani H, O'Connor GT, et al. Six-
907 Year Follow-up of a Trial of Antenatal Vitamin D for Asthma Reduction. N Engl J Med
908 [Internet]. 2020 Feb 6 [cited 2023 Jan 19];382(6):525–33. Available from:
909 https://www.nejm.org/doi/full/10.1056/NEJMoa1906137

910 14. Wolsk HM, Chawes BL, Litonjua AA, Hollis BW, Waage J, Stokholm J, et al. Prenatal
911 vitamin D supplementation reduces risk of asthma/recurrent wheeze in early childhood: A
912 combined analysis of two randomized controlled trials. PLoS One [Internet]. 2017 Oct 1
913 [cited 2023 Sep 25];12(10). Available from: https://pubmed.ncbi.nlm.nih.gov/29077711/

914 15. Wolsk HM, Harshfield BJ, Laranjo N, Carey VJ, O'Connor G, Sandel M, et al. Vitamin D
915 supplementation in pregnancy, prenatal 25(OH)D levels, race, and subsequent asthma or
916 recurrent wheeze in offspring: Secondary analyses from the Vitamin D Antenatal Asthma

917 Reduction Trial. J Allergy Clin Immunol [Internet]. 2017 Nov 1 [cited 2023 Sep
918 25];140(5):1423-1429.e5. Available from: https://pubmed.ncbi.nlm.nih.gov/28285844/

919 16. Verlaan DJ, Berlivet S, Hunninghake GM, Madore AM, Larivière M, Moussette S, et al.
920 Allele-specific chromatin remodeling in the ZPBP2/GSDMB/ORMDL3 locus associated
921 with the risk of asthma and autoimmune disease. Am J Hum Genet [Internet]. 2009 Sep 11
922 [cited 2022 Dec 13];85(3):377–93. Available from:
923 https://pubmed.ncbi.nlm.nih.gov/19732864/

924 17. Miller M, Rosenthal P, Beppu A, Mueller JL, Hoffman HM, Tam AB, et al. ORMDL3
925 transgenic mice have increased airway remodeling and airway responsiveness
926 characteristic of asthma. J Immunol [Internet]. 2014 Apr 15 [cited 2022 Dec
927 8];192(8):3475–87. Available from: https://pubmed.ncbi.nlm.nih.gov/24623133/

928 18. Zhang Y, Willis-Owen SAG, Spiegel S, Lloyd CM, Moffatt MF, Cookson WOCM. The
929 ORMDL3 Asthma Gene Regulates ICAM1 and Has Multiple Effects on Cellular
930 Inflammation. Am J Respir Crit Care Med [Internet]. 2019 Feb 15 [cited 2023 Sep
931 25];199(4):478–88. Available from: https://pubmed.ncbi.nlm.nih.gov/30339462/

932 19. Fishilevich S, Nudel R, Rappaport N, Hadar R, Plaschkes I, Stein TI, et al. GeneHancer:
933 genome-wide integration of enhancers and target genes in GeneCards. Database (Oxford)
934 [Internet]. 2017 [cited 2023 Sep 25];2017. Available from:
935 https://pubmed.ncbi.nlm.nih.gov/28605766/

936 20. Neme A, Seuter S, Carlberg C. Vitamin D-dependent chromatin association of CTCF in
937 human monocytes. Biochim Biophys Acta [Internet]. 2016 Nov 1 [cited 2023 Sep
938 25];1859(11):1380–8. Available from: https://pubmed.ncbi.nlm.nih.gov/27569350/

939 21. Neme A, Seuter S, Carlberg C. Selective regulation of biological processes by vitamin D
940 based on the spatio-temporal cistrome of its receptor. Biochim Biophys acta Gene Regul
941 Mech [Internet]. 2017 Sep 1 [cited 2023 Sep 25];1860(9):952–61. Available from:
942 https://pubmed.ncbi.nlm.nih.gov/28712921/

943 22. Ramagopalan S V., Heger A, Berlanga AJ, Maugeri NJ, Lincoln MR, Burrell A, et al. A
944 ChIP-seq defined genome-wide map of vitamin D receptor binding: associations with
945 disease and evolution. Genome Res [Internet]. 2010 Oct [cited 2023 Sep 25];20(10):1352–
946 60. Available from: https://pubmed.ncbi.nlm.nih.gov/20736230/

947 23. Lu X, Chu CS, Fang T, Rayon-Estrada V, Fang F, Patke A, et al. MTA2/NuRD Regulates
948 B Cell Development and Cooperates with OCA-B in Controlling the Pre-B to Immature B
949 Cell Transition. Cell Rep [Internet]. 2019 Jul 9 [cited 2023 Sep 25];28(2):472-485.e5.
950 Available from: https://pubmed.ncbi.nlm.nih.gov/31291582/

951 24. Buniello A, Macarthur JAL, Cerezo M, Harris LW, Hayhurst J, Malangone C, et al. The
952 NHGRI-EBI GWAS Catalog of published genome-wide association studies, targeted
953 arrays and summary statistics 2019. Nucleic Acids Res [Internet]. 2019 Jan 8 [cited 2023
954 Sep 25];47(D1):D1005–12. Available from: https://pubmed.ncbi.nlm.nih.gov/30445434/

955 25. Dobin A, Davis CA, Schlesinger F, Drenkow J, Zaleski C, Jha S, et al. STAR: ultrafast
956 universal RNA-seq aligner. Bioinformatics [Internet]. 2013 Jan [cited 2023 Sep
957 25];29(1):15–21. Available from: https://pubmed.ncbi.nlm.nih.gov/23104886/

958 26. Anders S, Pyl PT, Huber W. HTSeq—a Python framework to work with high-throughput
959 sequencing data. Bioinformatics [Internet]. 2015 Jan 15 [cited 2023 Sep 25];31(2):166–9.
960 Available from: https://dx.doi.org/10.1093/bioinformatics/btu638

961 27. McCarthy DJ, Chen Y, Smyth GK. Differential expression analysis of multifactor RNA-
962 Seq experiments with respect to biological variation. Nucleic Acids Res [Internet]. 2012
963 May [cited 2023 Sep 25];40(10):4288. Available from: /pmc/articles/PMC3378882/

964 28. Sakai Y, Kishimoto J, Demay MB. Metabolic and cellular analysis of alopecia in vitamin
965 D receptor knockout mice. J Clin Invest [Internet]. 2001 [cited 2023 Sep 25];107(8):961–
966 6. Available from: https://pubmed.ncbi.nlm.nih.gov/11306599/

967 29. Li YC, Amling M, Pirro AE, Priemel M, Meuse J, Baron R, et al. Normalization of
968 mineral ion homeostasis by dietary means prevents hyperparathyroidism, rickets, and
969 osteomalacia, but not alopecia in vitamin D receptor-ablated mice. Endocrinology
970 [Internet]. 1998 [cited 2023 Sep 25];139(10):4391–6. Available from:
971 https://pubmed.ncbi.nlm.nih.gov/9751523/

972 30. Love MI, Huber W, Anders S. Moderated estimation of fold change and dispersion for
973 RNA-seq data with DESeq2. Genome Biol [Internet]. 2014 Dec 5 [cited 2023 Sep
974 25];15(12):1–21. Available from:
975 https://genomebiology.biomedcentral.com/articles/10.1186/s13059-014-0550-8

976 31. Yu G, Wang LG, Han Y, He QY. clusterProfiler: an R package for comparing biological
977 themes among gene clusters. OMICS [Internet]. 2012 May 1 [cited 2023 Sep
978 25];16(5):284–7. Available from: https://pubmed.ncbi.nlm.nih.gov/22455463/

979 32. Ritchie ME, Phipson B, Wu D, Hu Y, Law CW, Shi W, et al. limma powers differential
980 expression analyses for RNA-sequencing and microarray studies. Nucleic Acids Res
981 [Internet]. 2015 Apr 20 [cited 2018 Feb 18];43(7):e47–e47. Available from:
982 http://academic.oup.com/nar/article/43/7/e47/2414268/limma-powers-differential-

983 expression-analyses-for

984 33. Benjamini Y, Drai D, Elmer G, Kafkafi N, Golani I. Controlling the false discovery rate in
985 behavior genetics research. Behav Brain Res [Internet]. 2001 Nov 8 [cited 2023 Sep
986 25];125(1–2):279–84. Available from: https://pubmed.ncbi.nlm.nih.gov/11682119/

987 34. Silverbush D, Sharan R. A systematic approach to orient the human protein-protein
988 interaction network. Nat Commun [Internet]. 2019 Dec 1 [cited 2022 Mar 15];10(1).
989 Available from: https://pubmed-ncbi-nlm-nih-gov.ezp-prod1.hul.harvard.edu/31289271/

990 35. Smedley D, Haider S, Durinck S, Pandini L, Provero P, Allen J, et al. The BioMart
991 community portal: an innovative alternative to large, centralized data repositories. Nucleic
992 Acids Res [Internet]. 2015 [cited 2023 Sep 25];43(W1):W589–98. Available from:
993 https://pubmed.ncbi.nlm.nih.gov/25897122/

994 36. Moffatt MF, Kabesch M, Liang L, Dixon AL, Strachan D, Heath S, et al. Genetic variants
995 regulating ORMDL3 expression contribute to the risk of childhood asthma. Nature
996 [Internet]. 2007 Jul 26 [cited 2022 Dec 8];448(7152):470–3. Available from:
997 https://pubmed.ncbi.nlm.nih.gov/17611496/

998 37. Litherland SA, Xie TX, Grebe KM, Davoodi-Semiromi A, Elf J, Belkin NS, et al. Signal
999 transduction activator of transcription 5 (STAT5) dysfunction in autoimmune monocytes
1000 and macrophages. J Autoimmun [Internet]. 2005 Jun [cited 2023 Sep 25];24(4):297.
1001 Available from: /pmc/articles/PMC2605968/

1002 38. Kara S, Pirela-Morillo GA, Gilliam CT, Wilson GD. Identification of novel susceptibility
1003 genes associated with seven autoimmune disorders using whole genome molecular
1004 interaction networks. J Autoimmun [Internet]. 2019 Feb 1 [cited 2023 Sep 25];97:48–58.

1005 Available from: https://pubmed.ncbi.nlm.nih.gov/30391024/

1006 39. Syreeni A, Sandholm N, Sidore C, Cucca F, Haukka J, Harjutsalo V, et al. Genome-wide
1007 search for genes affecting the age at diagnosis of type 1 diabetes. J Intern Med [Internet].
1008 2021 May 1 [cited 2023 Sep 25];289(5):662–74. Available from:
1009 https://pubmed.ncbi.nlm.nih.gov/33179336/

1010 40. Shrine N, Portelli MA, John C, Soler Artigas M, Bennett N, Hall R, et al. Moderate-to-
1011 severe asthma in individuals of European ancestry: a genome-wide association study.
1012 Lancet Respir Med [Internet]. 2019 Jan 1 [cited 2023 Sep 25];7(1):20. Available from:
1013 /pmc/articles/PMC6314966/

1014 41. Marinho S, Custovic A, Marsden P, Smith JA, Simpson A. 17q12-21 variants are
1015 associated with asthma and interact with active smoking in an adult population from the
1016 United Kingdom. Ann Allergy Asthma Immunol [Internet]. 2012 [cited 2022 Dec
1017 8];108(6). Available from: https://pubmed.ncbi.nlm.nih.gov/22626592/

1018 42. Hitomi Y, Kojima K, Kawashima M, Kawai Y, Nishida N, Aiba Y, et al. Identification of
1019 the functional variant driving ORMDL3 and GSDMB expression in human chromosome
1020 17q12-21 in primary biliary cholangitis. Sci Rep [Internet]. 2017 Dec 1 [cited 2023 Sep
1021 25];7(1). Available from: /pmc/articles/PMC5460198/

1022 43. Keshari PK, Harbo HF, Myhr KM, Aarseth JH, Bos SD, Berge T. Allelic imbalance of
1023 multiple sclerosis susceptibility genes IKZF3 and IQGAP1 in human peripheral blood.
1024 BMC Genet [Internet]. 2016 Apr 14 [cited 2023 Sep 25];17(1). Available from:
1025 https://pubmed.ncbi.nlm.nih.gov/27080863/

1026 44. Quintana FJ, Jin H, Burns EJ, Nadeau M, Yeste A, Kumar D, et al. Aiolos promotes TH17

1027 differentiation by directly silencing Il2 expression. Nat Immunol [Internet]. 2012 Aug
1028 [cited 2023 Sep 25];13(8):770–7. Available from:
1029 https://pubmed.ncbi.nlm.nih.gov/22751139/

1030 45. Pfeffer PE, Hawrylowicz CM. Vitamin D in Asthma: Mechanisms of Action and
1031 Considerations for Clinical Trials. Chest [Internet]. 2018 May 1 [cited 2023 Sep
1032 25];153(5):1229–39. Available from: https://pubmed.ncbi.nlm.nih.gov/28923762/

1033 46. Baeke F, Korf H, Overbergh L, van Etten E, Verstuyf A, Gysemans C, et al. Human T
1034 lymphocytes are direct targets of 1,25-dihydroxyvitamin D3 in the immune system. J
1035 Steroid Biochem Mol Biol [Internet]. 2010 Jul [cited 2023 Sep 25];121(1–2):221–7.
1036 Available from: https://pubmed.ncbi.nlm.nih.gov/20302932/

1037 47. Zhu J, Cote-Sierra J, Guo L, Paul WE. Stat5 activation plays a critical role in Th2
1038 differentiation. Immunity [Internet]. 2003 [cited 2023 Sep 25];19(5):739–48. Available
1039 from: https://pubmed.ncbi.nlm.nih.gov/14614860/

1040 48. Boonstra A, Barrat FJ, Crain C, Heath VL, Savelkoul HFJ, O'Garra A. 1alpha,25-
1041 Dihydroxyvitamin d3 has a direct effect on naive CD4(+) T cells to enhance the
1042 development of Th2 cells. J Immunol [Internet]. 2001 Nov 1 [cited 2023 Sep
1043 25];167(9):4974–80. Available from: https://pubmed.ncbi.nlm.nih.gov/11673504/

1044 49. Cantorna MT, Snyder L, Lin YD, Yang L. Vitamin D and 1,25(OH)2D regulation of T
1045 cells. Nutrients [Internet]. 2015 Apr 22 [cited 2023 Sep 25];7(4):3011–21. Available from:
1046 https://pubmed.ncbi.nlm.nih.gov/25912039/

1047 50. Pichler J, Gerstmayr M, Szépfalusi Z, Urbanek R, Peterlik M, Willheim M. 1
1048 alpha,25(OH)2D3 inhibits not only Th1 but also Th2 differentiation in human cord blood

1049 T cells. Pediatr Res [Internet]. 2002 Jul [cited 2023 Sep 25];52(1):12–8. Available from:
1050 https://pubmed.ncbi.nlm.nih.gov/12084841/

1051 51. Staeva-Vieira TP, Freedman LP. 1,25-dihydroxyvitamin D3 inhibits IFN-gamma and IL-4
1052 levels during in vitro polarization of primary murine CD4+ T cells. J Immunol [Internet].
1053 2002 Feb 1 [cited 2023 Sep 25];168(3):1181–9. Available from:
1054 https://pubmed.ncbi.nlm.nih.gov/11801653/

1055

1056

1057

1058 **Appendix 1**

1059 **Primer sequences**

Gene	**species**	**sequence**
Gsdma antisense	mouse	5'-TCA ACC AGC TTC AGT TGC AC-3'
Gsdma sense	mouse	5'-TGC TGT CAA AGG ACG CTA TG-3'
Ikzf3 sense	mouse	5'-TGT CAC CTC TGC AAC TAC GC-3'
Ikzsf3 antisense	mouse	5'-TTC CGC AGA ACT CAC ACT TG-3'
IL-2 antisense	mouse	5'-ATC CTG GGG AGT TTC AGG TT-3'
IL-2 sense	mouse	5'-CCC ACT TCA AGC TCC ACT TC-3'
Ormdl3 antisense	mouse	5'-CTT TGC CTT GGT CTG GAG TC-3'
Ormdl3 sense	mouse	5'-CAC ACG GGT GAT GAA C AG TC-3'
Stat3 antisense	mouse	5'-TCG TGG TAA ACT GGA CAC CA-3'

Stat3 sense	mouse	5'-GAG GAG CTG CAG CAG AAA GT-3'
Stat5a antisense	mouse	5'-GTC AAA CTC GCC ATC TTG GT-3'
Stat5a sense	mouse	5'-TAC ATG GAC CAG GCT CCT TC-3'
Stat5b antisense	mouse	5'-TGG GTG GCC TTA ATG TTC TC-3'
Stat5b sense	mouse	5'-TGT GGA TAC AGG CTC AGC AG-3'

1060

1061

1062 **Appendix 2**

1063 **Antibodies**

Antibody	**clone**	**Vendor**	**catalog #**
Aiolos PE	8B2	Biolegend	653204
CD122 (IL2Rβ) APC	5H4	Biolegend	5H4
CD19 PE-Cy7	6D5	Biolegend	115520
CD4 FITC	RM4-5	Biolegend	100510
CD4 PerCPeFluor710	RM4-5	eBioscience	46-0042-82
CD44 FITC	IM7	Biolegend	103006
CD45 BV421	104	Biolegend	109832
CD62L PE	MEL-14	Biolegend	104408
CD8a APC-Cy7	53-6.7	Biolegend	100714
Foxp3 PE	FJK-16s	Invitrogen	12-5773-82
Gata3 PE	16E10A23	Biolegend	653804
IFNg FITC	XMG1.2	Biolegend	505806
IL-10 Pacific Blue	JES5-16E3	Biolegend	505020

IL-13 eFluor660	eBio13A	eBioscience	50-7133-82
IL-13 PE	eBio13A	molecular probes	A18492
IL17A PE-Cy7	TC11-18H10.1	Biolegend	506922
IL-2 PE-TexasRed	JES6-5H4	Biolegend	503840
monoclonal b-actin-Peroxidase	AC-15	Sigma-Aldrich	A3854
Phospho-BTK/ITK	M4G3LN	eBioscience	12-9015-42
Tbet PE	4B10	Biolegend	644809
VDR	D2K6W	Cell Signaling Technology	12550S
VDR AlexaFluor647	D2K6W	Cell Signaling Technology	custom order

1064

1065 **Appendix 3**

Reagent	**Vendor**	**catalog #**
anti-mouse CD28 (37.51)	BD Biosciences	553294
anti-mouse CD3e (145-2C11)	BD Biosciences	553057
b-mercaptoethanol	gibco	21985-032
calcitriol	Sigma-Aldrich	D1530
collagenase D	Roche	11088866001
Kwik-Diff soultion	Shandon	9990700
DMSO	Sigma-Aldrich	D2438
ProLong gold Anitfade Mountant with DAPI	ThermoFisher Scietific	P36935
rat anti-mouse anti-IFNg	BD Biosciences	554430
Anti-Mouse CD16/CD32 (Mouse BD Fc Block	BD Biosciences	553141
hamster anti-mouse anti-IL-4 (11B11)	BD Biosciences	554433

L-Glutamin	Sigma- Aldrich	G7513
LS columns	Miltenyi	130-042-401
microRNeasy	Qiagen	74004
naive CD4+ T cell isolation kit	Miltenyi	130-104-453
MEM non-essential amino acid solution (100x)	Sigma- Aldrich	M7145
Penicillin/Streptomycin	Sigma- Aldrich	P4333
Cell stimulation Cocktail (500x) phorbol myristate acetate (PMA)/Ionomycin	Tocris	TNB-4975
phosphate buffered saline	Gibco	14190-144
recombinant human TGFb1	Peprotech	100-21C
recombinant mouse IL-12	Peprotech	210-12
recombinant mouse IL-13	Peprotech	210-13
recombinant mouse IL-2	Peprotech	212-12
recombinant mouse IL-33	Peprotech	210-33
recombinant mouse IL-4	Peprotech	214-14
recombinant mouse IL-6	Peprotech	216-16
recombinant human IL-2	Peprotech	200-02
RPMI1640	Sigma-Aldrich	R8758
STAT3 inhibitor III WP1066	Sigma-Aldrich	573129
STAT5 inhibitor	EMD Millipore	573106
AS1517499 (STAT6 inhibitor)	Millipore-Sigma	SML190
U0126	CellSignaling Technologies	9903S

LY294002	CellSignaling Technologies	9901S
SsoFast Eva Green	Bio-Rad	1725201
10x zink fixative	BD Pharmingen	552658
Tris-Glycine-SDS Running Buffer	Boston Bioproducts	BP-150
Transfer buffer	Boston Bioproducts	BP-190
Tris Buffered Saline with Tween 20	CellSignaling Technologies	9997S

1066

Vitamin D constrains inflammation by modulating the expression of key genes on Chr17q12-21.1

Authors:
Ayşe Kılıç[1*], Arda Halu[1*], Margherita De Marzio[1,2], Enrico Maiorino[1], Melody G. Duvall[3], Thayse Brueggemann[3], Joselyn J. Rojas Quintero[3], Robert Chase[1], Hooman Mirzakhani[1], Ayse Özge Sungur[4, 5], Janine Koepke[5], Taiji Nakano[6], Hong Yong Peh[3], Nandini Krishnamoorthy[3], Raja-Elie Abdulnour[3], Katia Georgopoulos[7], Augusto A. Litonjua[8], Marie B. Demay[9], Harald Renz[10,11], Bruce D. Levy[3] and Scott T. Weiss[1*]

Affiliations:
1 Channing Division of Network Medicine, Department of Medicine, Brigham and Women's Hospital and Harvard Medical School; Boston, MA, USA.
2 Department of Environmental Health, Harvard TH Chan School of Public Health; Boston, MA, USA.
3 Division of Pulmonary and Critical Care Medicine, Department of Medicine, Brigham and Women's Hospital and Harvard Medical School; Boston, MA, USA.
4 Behavioral Neuroscience, Experimental and Biological Psychology, Philipps-University Marburg; Marburg, Germany.
5 Excellence Cluster Cardio-Pulmonary System (ECCPS), Justus Liebig University Giessen; Giessen, Germany.
6 Department of Pediatrics, Graduate School of Medicine, Chiba University; Chiba, Japan.
7 Cutaneous Biology Research Center, Massachusetts General Hospital and Harvard Medical School; Charlestown, Massachusetts, USA.
8 Division of Pediatric Pulmonary Medicine, Golisano Children's Hospital at Strong, University of Rochester Medical Center; Rochester, NY, USA.
9 Endocrine Unit, Massachusetts General Hospital and Harvard Medical School; Boston, MA, USA.
10 Institute of Laboratory Medicine and Pathobiochemistry, Molecular Diagnostics, Philipps University of Marburg and German Center for Lung Research (DZL); Marburg, Germany.
11 Department of Clinical Immunology and Allergology, Laboratory of Immunopathology Sechenov University; Moscow, Russia.

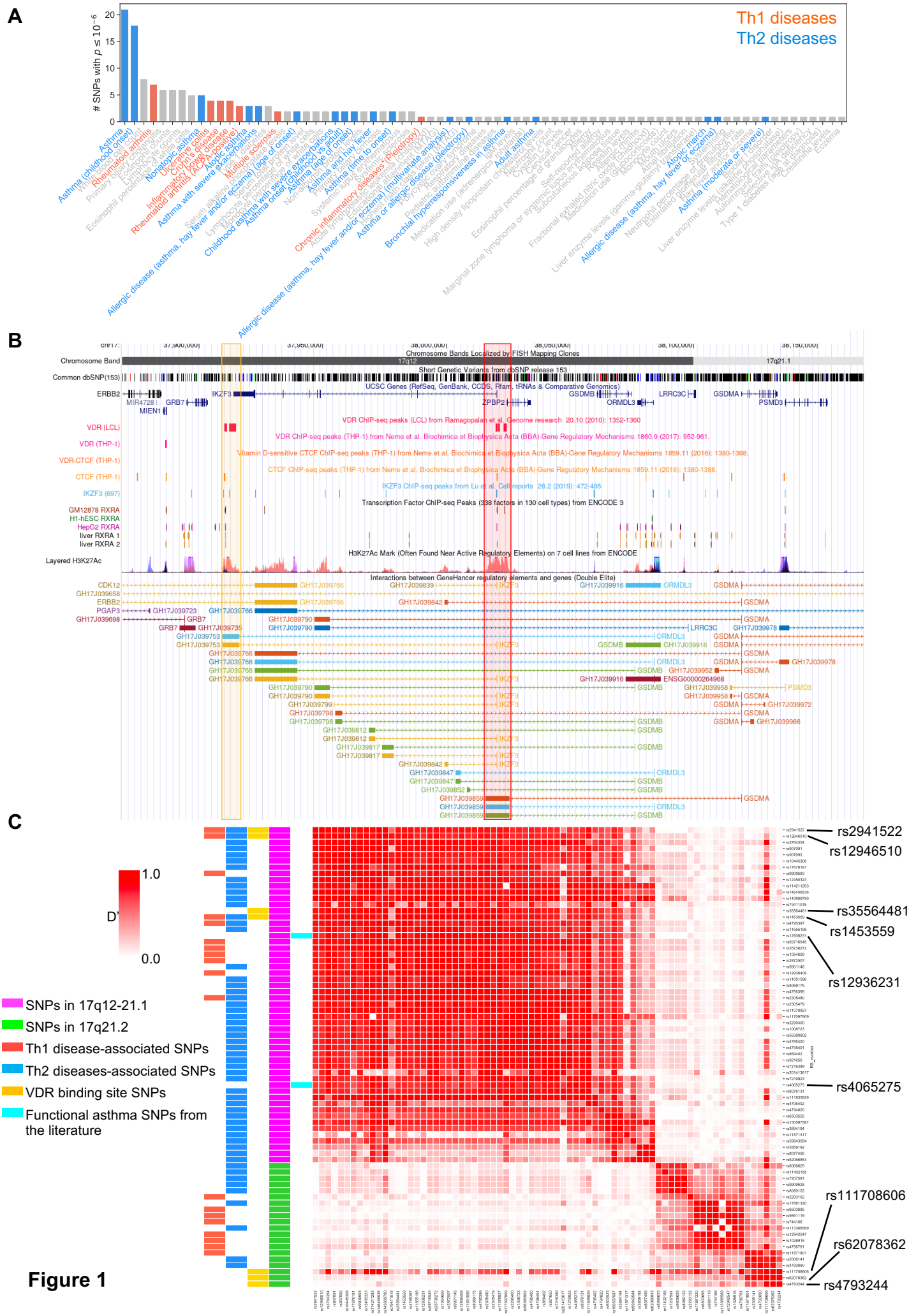
A
Th1 diseases
Th2 diseases
SNPs with p ≤ 10^-6
B
Chromosome Band
Common dbSNP(153)
UCSC Genes (RefSeq, GenBank, CCDS, Rfam, tRNAs & Comparative Genomics)
VDR (LCL)
VDR (THP-1)
VDR-CTCF (THP-1)
CTCF (THP-1)
IKZF3 (697)
Transcription Factor ChIP-seq Peaks (338 factors in 130 cell types) from ENCODE 3
Layered H3K27Ac
H3K27Ac Mark (Often Found Near Active Regulatory Elements) on 7 cell lines from ENCODE
Interactions between GeneHancer regulatory elements and genes (Double Elite)
C
D'
1.0
0.0
SNPs in 17q12-21.1
SNPs in 17q21.2
Th1 disease-associated SNPs
Th2 diseases-associated SNPs
VDR binding site SNPs
Functional asthma SNPs from the literature
rs2941522
rs12946510
rs35564481
rs1453559
rs12936231
rs4065275
rs111708606
rs62078362
rs4793244

Figure 1

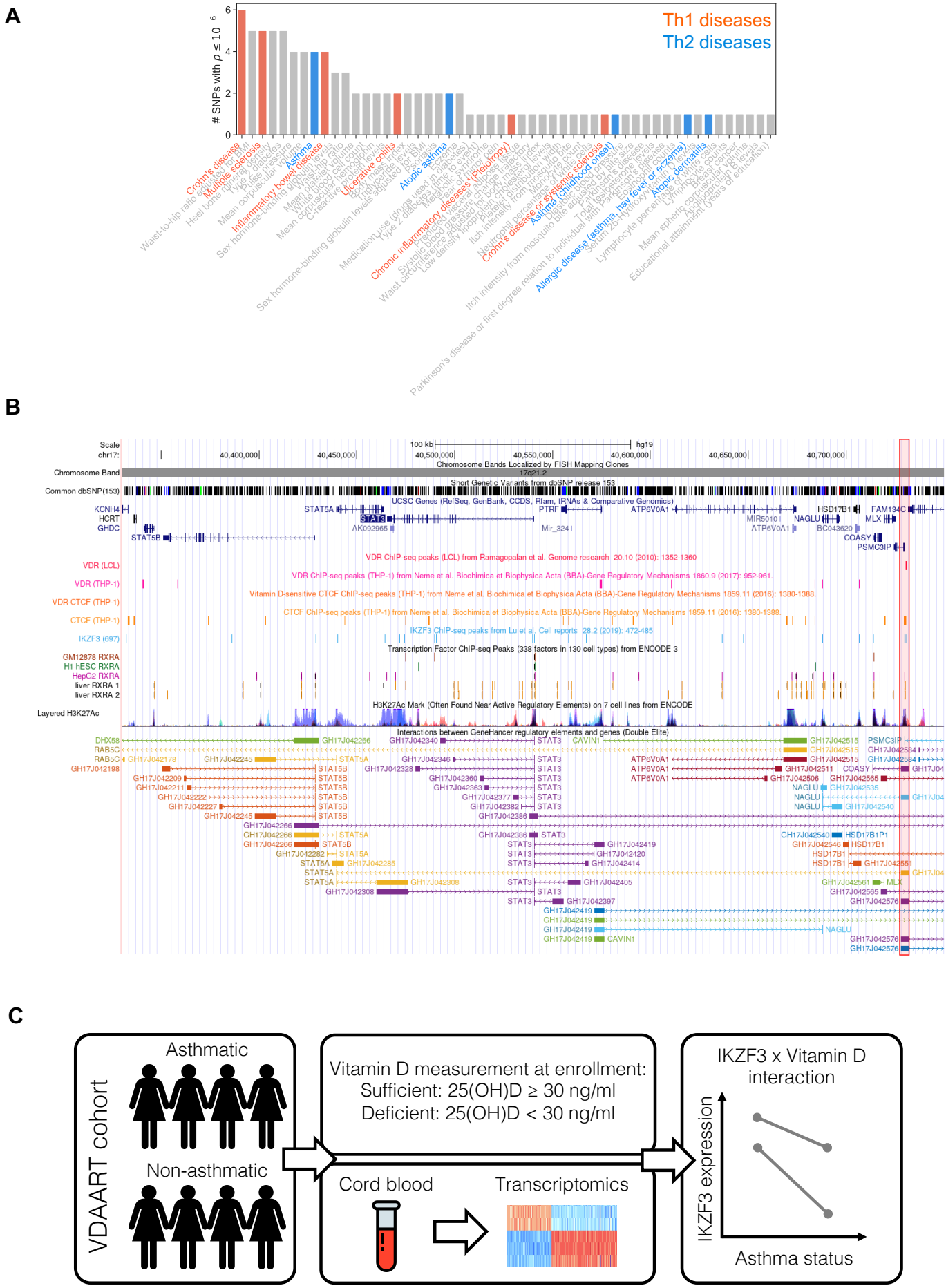

Figure 1-figure supplement 1

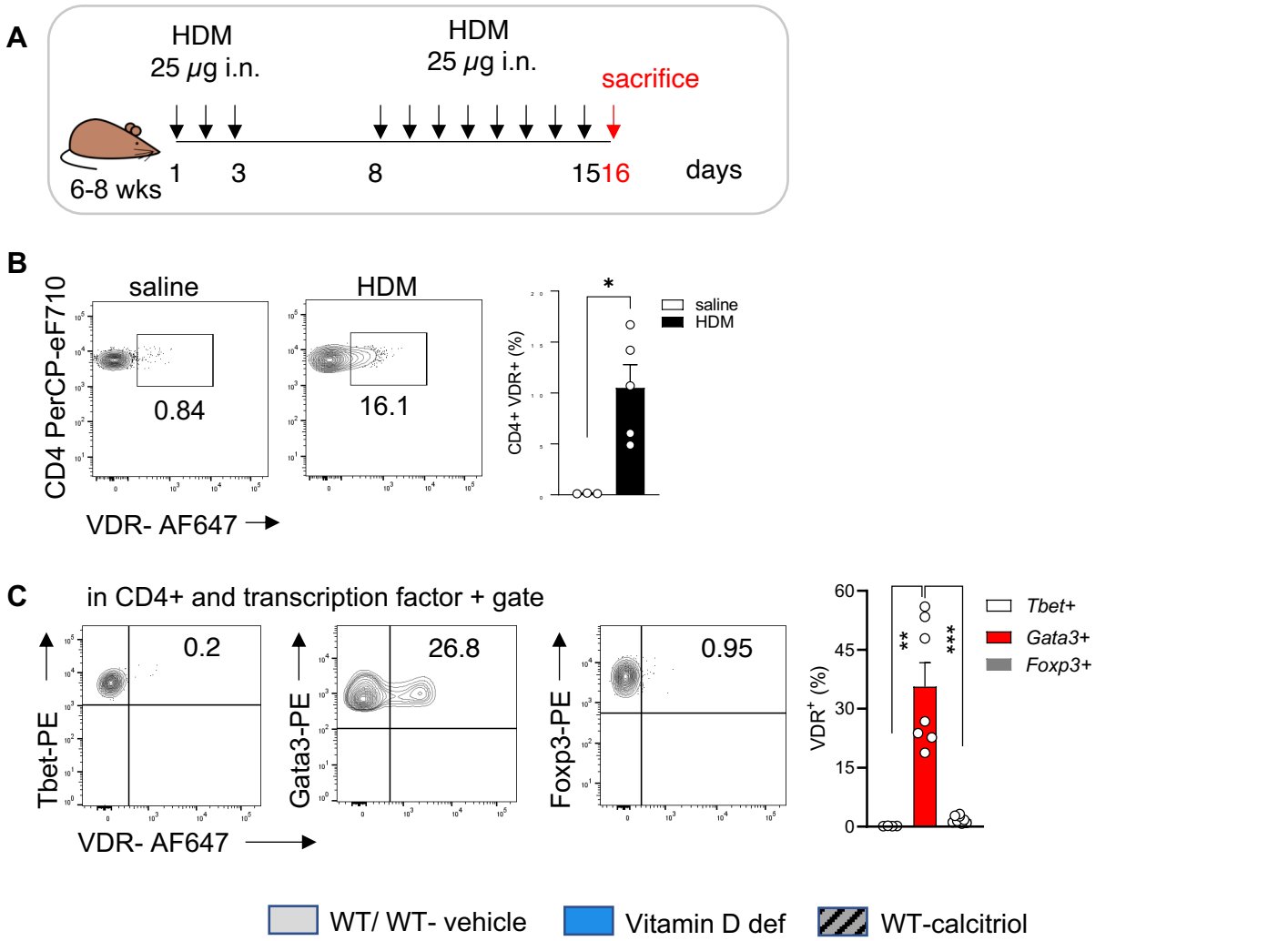
A
HDM
25 μg i.n.
HDM
25 μg i.n.
sacrifice
6-8 wks
1
3
8
15
16
days
B
saline
HDM
CD4 PerCP-eF710
0.84
16.1
VDR- AF647
CD4+ VDR+ (%)
saline
HDM
C
in CD4+ and transcription factor + gate
Tbet-PE
0.2
Gata3-PE
26.8
Foxp3-PE
0.95
VDR- AF647
VDR+ (%)
Tbet+
Gata3+
Foxp3+
WT/ WT- vehicle
Vitamin D def
WT-calcitriol
D
Ikzf3
Ormdl3
Gsdma
rel. mRNA expression
f
E
Stat5a
Stat5b
Stat3
ns
g

Figure 2

A gating strategy

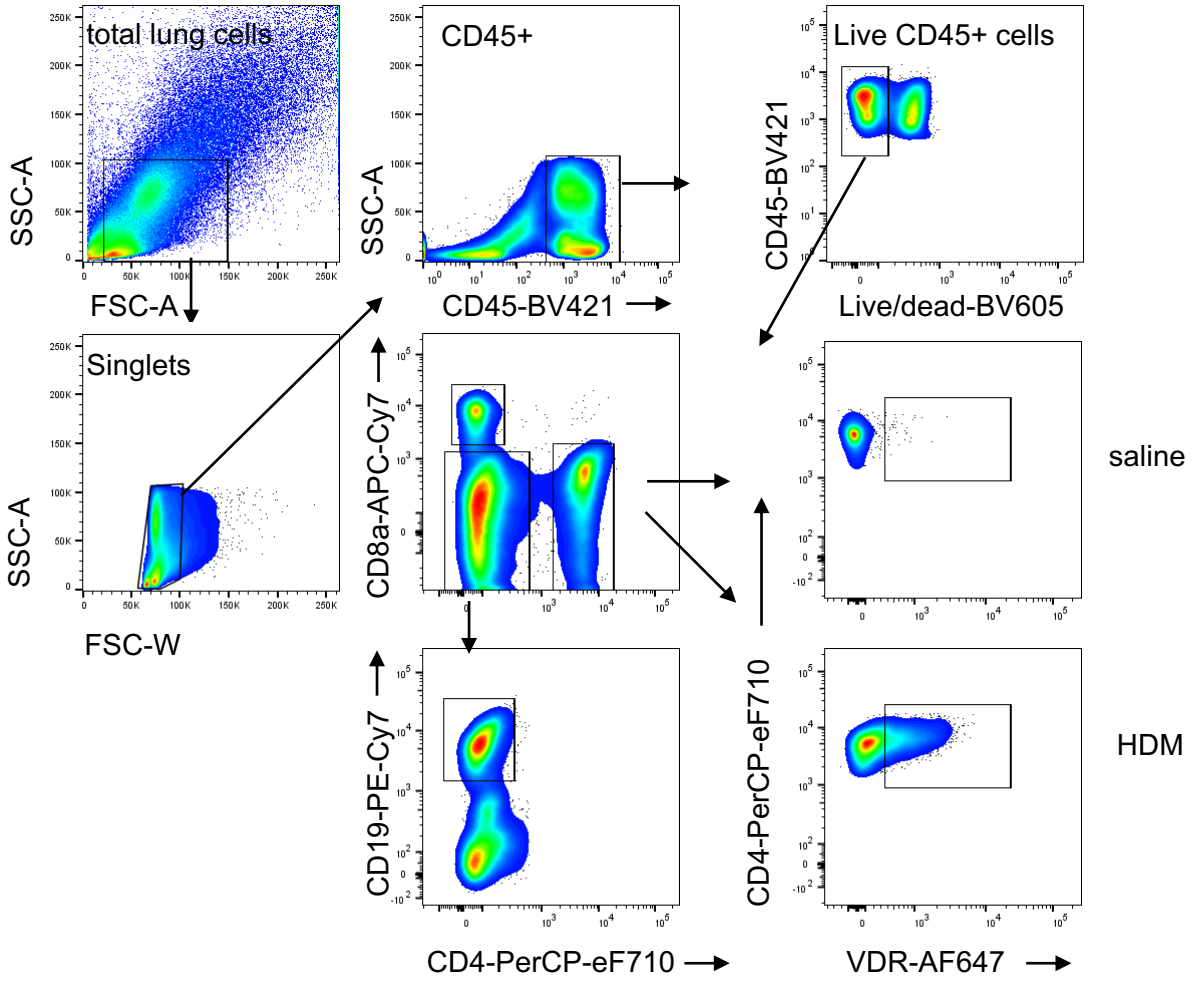

B

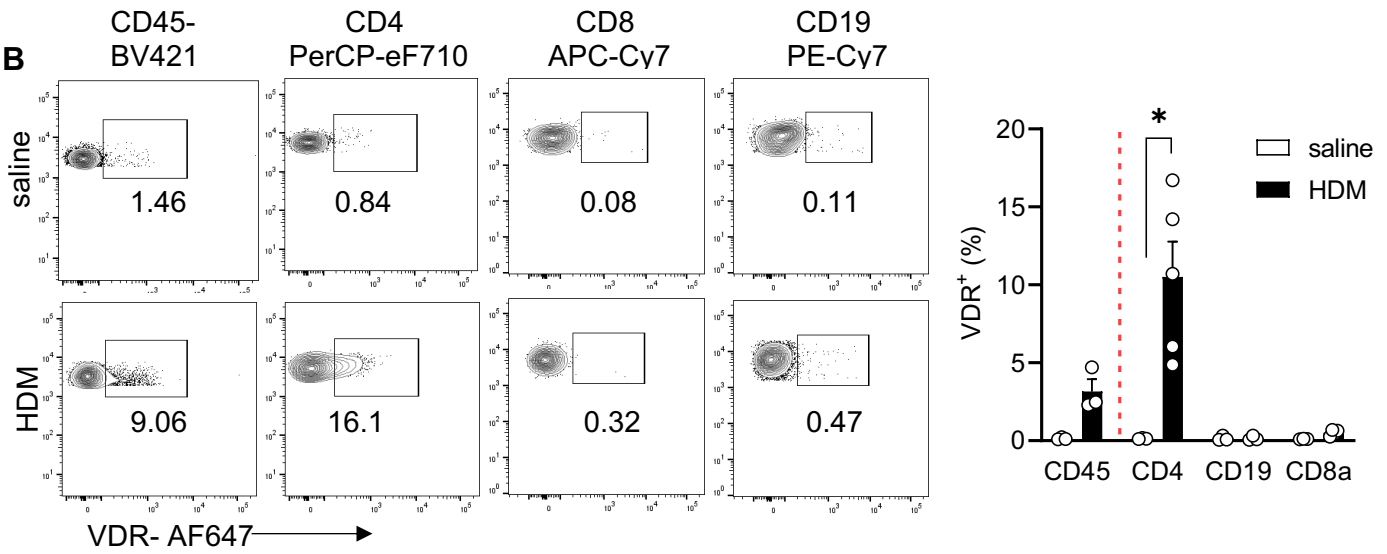

C gated on CD45+ CD4+

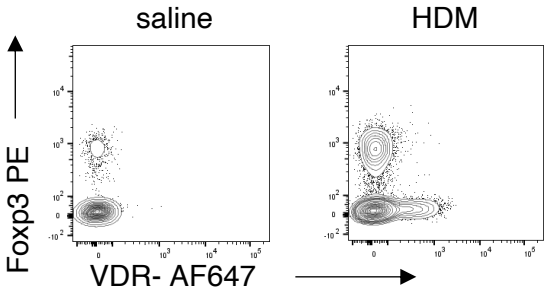

Figure 2 - figure supplement 1

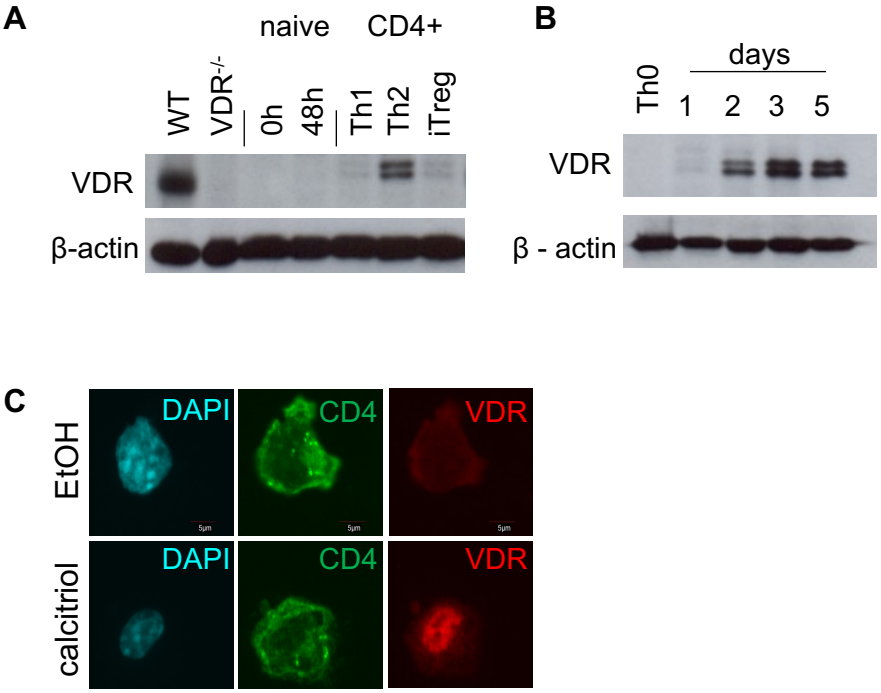

Figure 2 - figure supplement 2

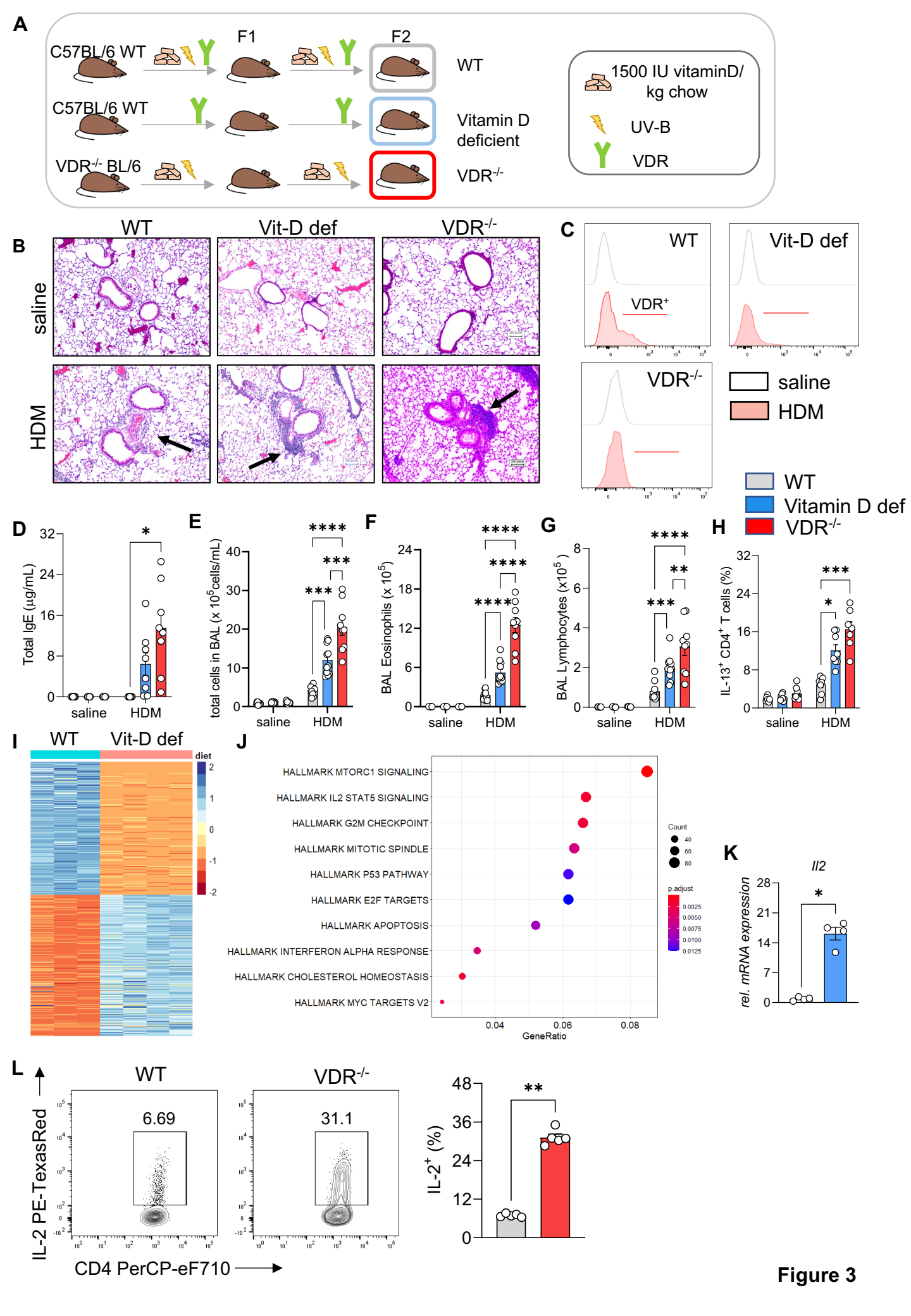
A
C57BL/6 WT
F1
F2
WT
C57BL/6 WT
Vitamin D deficient
VDR-/- BL/6
VDR-/-
1500 IU vitaminD/ kg chow
UV-B
VDR
B
WT
Vit-D def
VDR-/-
saline
HDM
C
WT
Vit-D def
VDR+
VDR-/-
saline
HDM
WT
Vitamin D def
VDR-/-
D
Total IgE (µg/mL)
saline
HDM
E
total cells in BAL (x 10^5 cells/mL)
F
BAL Eosinophils (x 10^5)
G
BAL Lymphocytes (x10^5)
H
IL-13+ CD4+ T cells (%)
I
WT
Vit-D def
diet
J
HALLMARK MTORC1 SIGNALING
HALLMARK IL2 STAT5 SIGNALING
HALLMARK G2M CHECKPOINT
HALLMARK MITOTIC SPINDLE
HALLMARK P53 PATHWAY
HALLMARK E2F TARGETS
HALLMARK APOPTOSIS
HALLMARK INTERFERON ALPHA RESPONSE
HALLMARK CHOLESTEROL HOMEOSTASIS
HALLMARK MYC TARGETS V2
GeneRatio
Count
p.adjust
K
Il2
rel. mRNA expression
L
WT
VDR-/-
6.69
31.1
IL-2 PE-TexasRed
CD4 PerCP-eF710
IL-2+ (%)

Figure 3

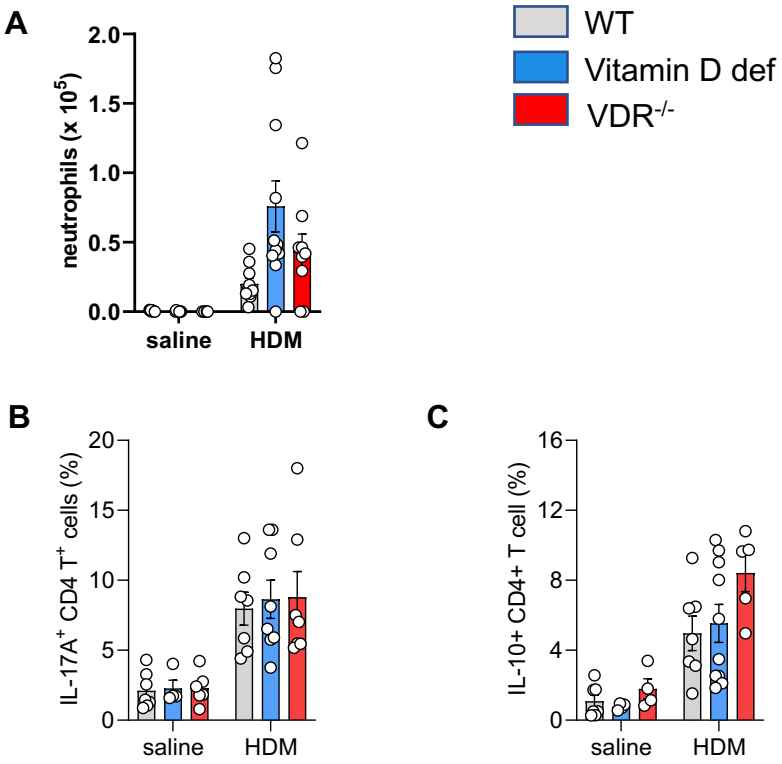

Figure 3 - figure supplement 1

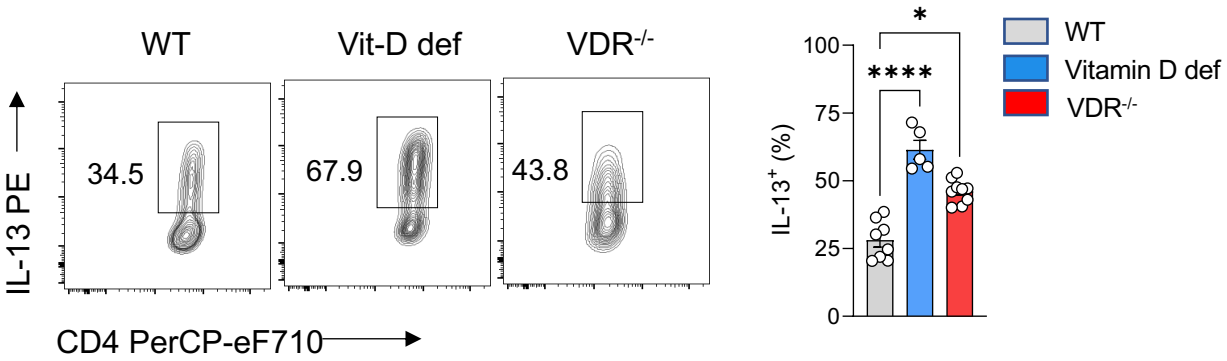

Figure 3 - figure supplement 2

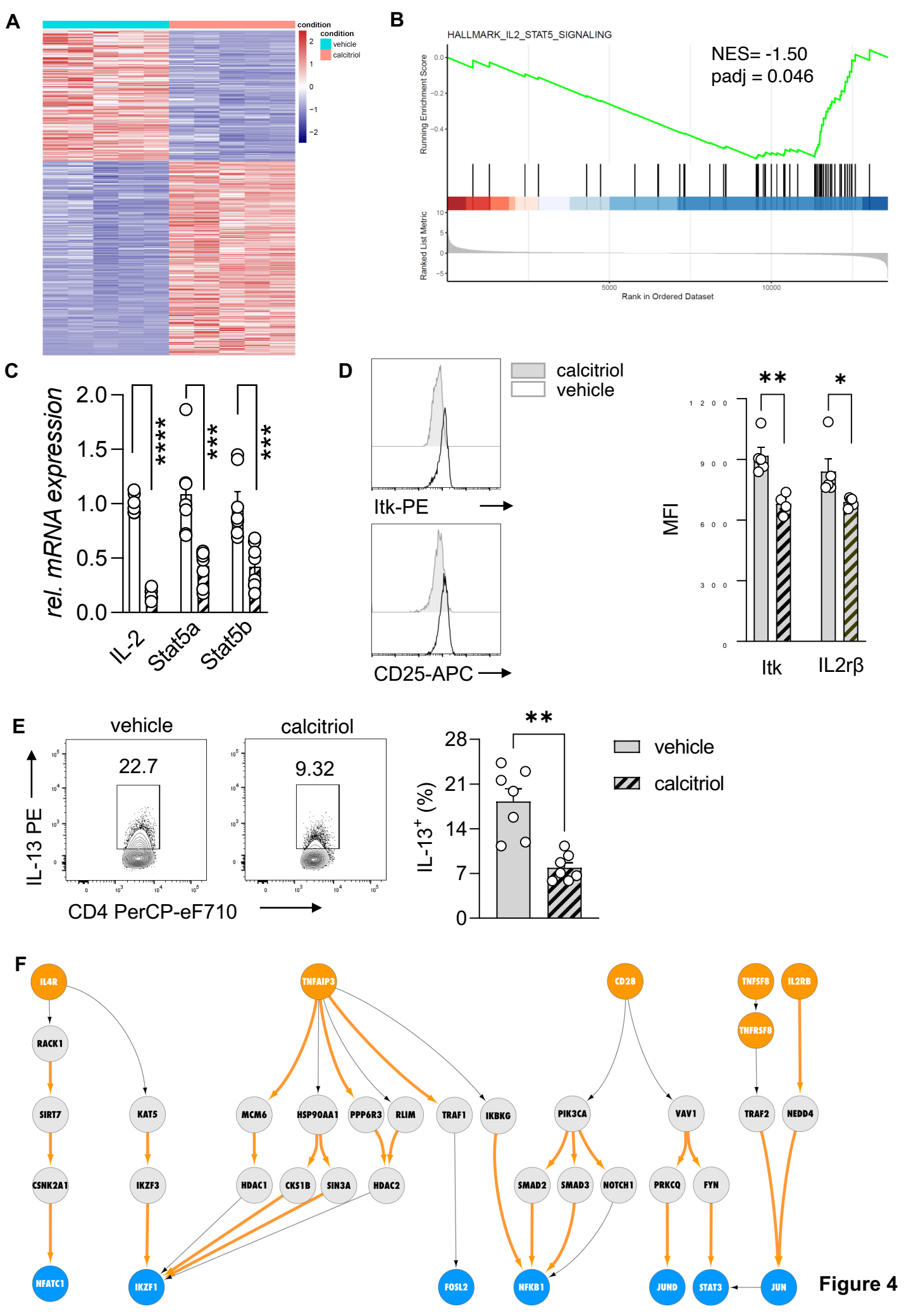
A
condition
vehicle
calcitriol
B
HALLMARK_IL2_STAT5_SIGNALING
NES= -1.50
padj = 0.046
Running Enrichment Score
Ranked List Metric
Rank in Ordered Dataset
C
rel. mRNA expression
IL-2
Stat5a
Stat5b
D
calcitriol
vehicle
Itk-PE
CD25-APC
MFI
Itk
IL2rβ
E
vehicle
calcitriol
22.7
9.32
IL-13 PE
CD4 PerCP-eF710
IL-13+ (%)
F
IL4R
RACK1
SIRT7
CSNK2A1
NFATC1
KAT5
IKZF3
IKZF1
TNFAIP3
MCM6
HSP90AA1
PPP6R3
RLIM
TRAF1
IKBKG
HDAC1
CKS1B
SIN3A
HDAC2
FOSL2
NFKB1
CD28
PIK3CA
SMAD2
SMAD3
NOTCH1
VAV1
PRKCQ
FYN
JUND
STAT3
TNFSF8
IL2RB
TNFRSF8
TRAF2
NEDD4
JUN

Figure 4

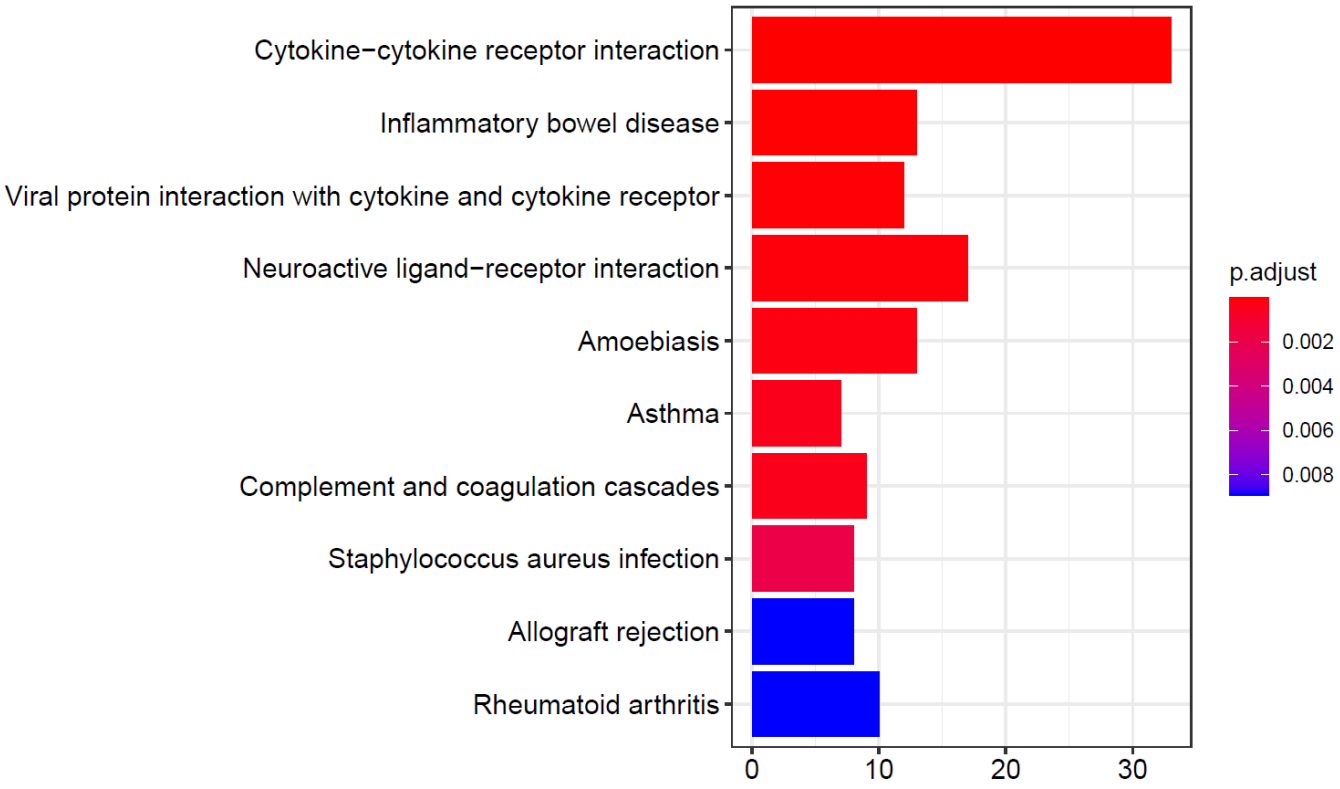

Figure 4 - figure supplement 1

A

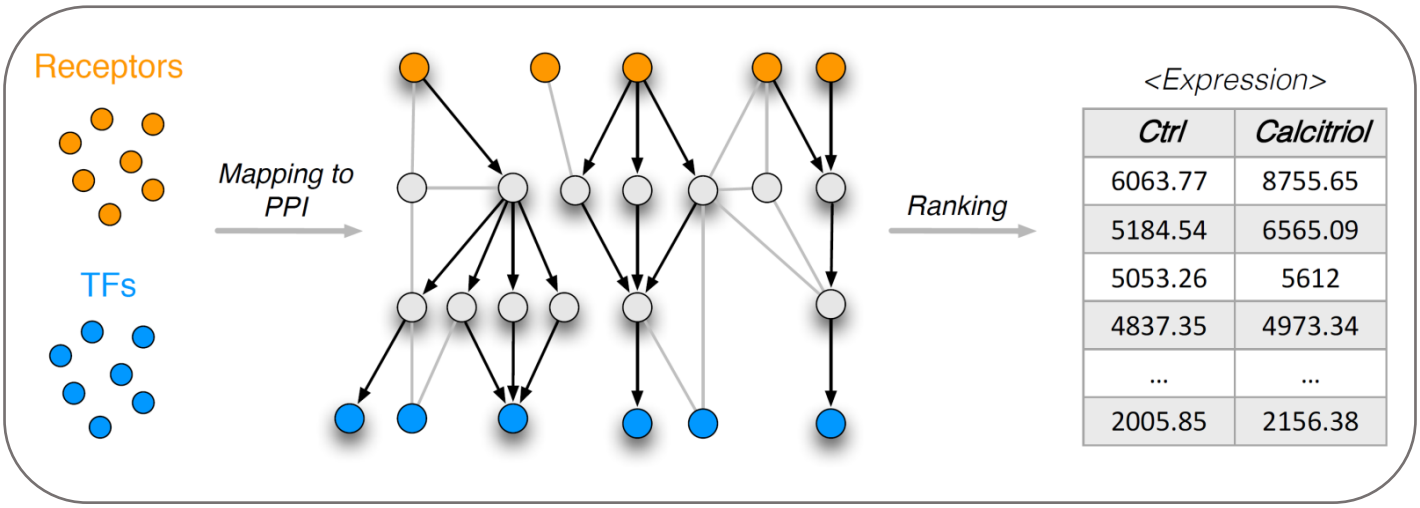

B

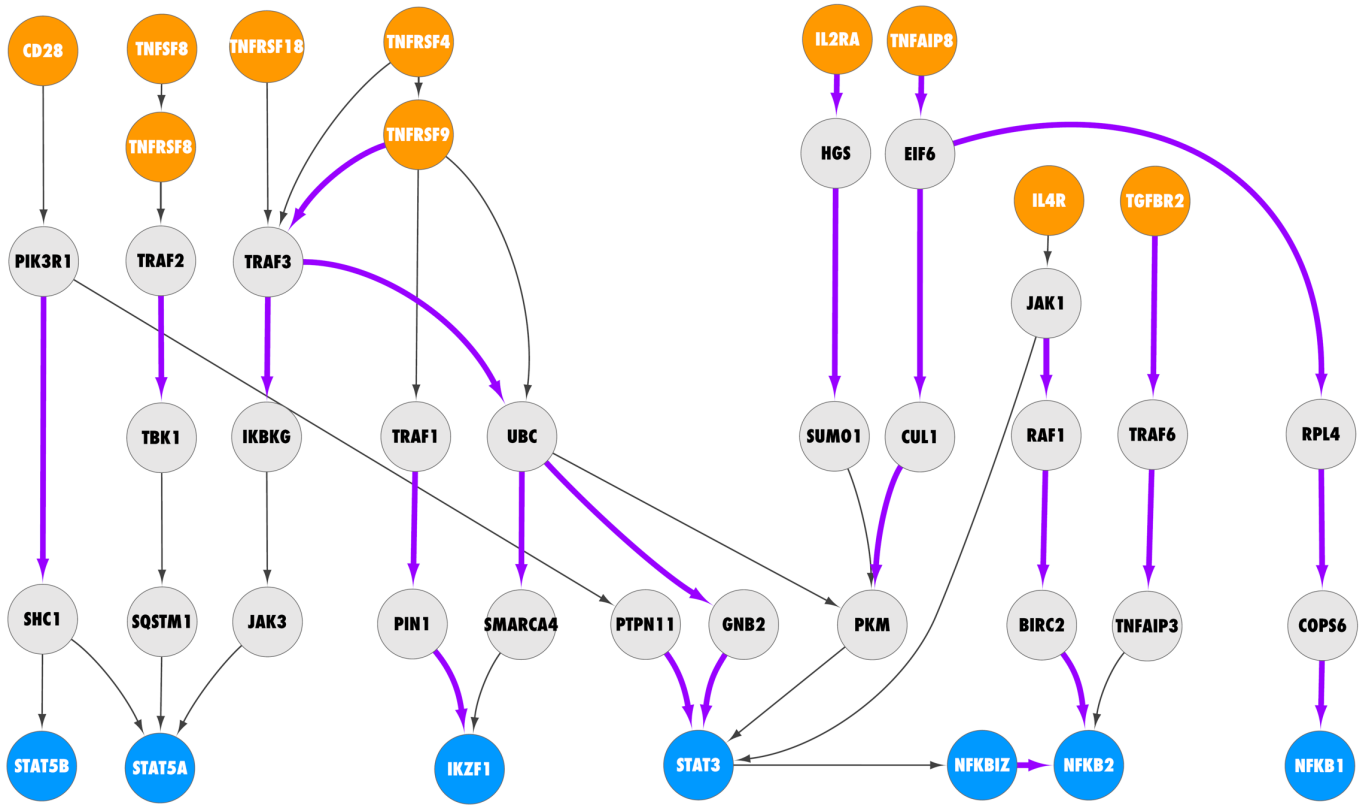

Figure 4 - figure supplement 2

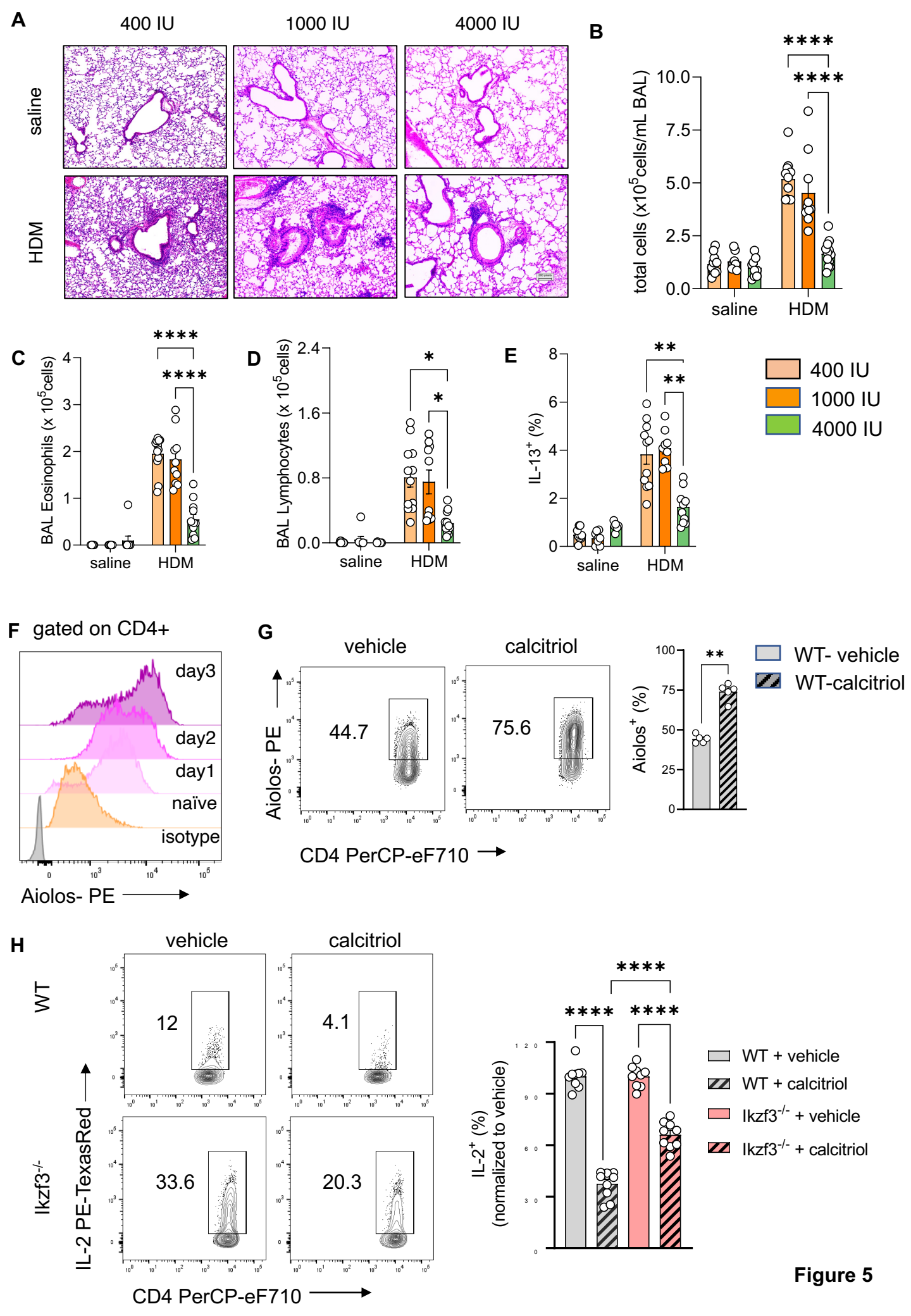
A
400 IU
1000 IU
4000 IU
saline
HDM
B
total cells (x10^5 cells/mL BAL)
10.0
7.5
5.0
2.5
0.0
saline
HDM
****
****
C
BAL Eosinophils (x 10^5 cells)
4
3
2
1
0
saline
HDM
****
****
D
BAL Lymphocytes (x 10^5 cells)
2.4
1.6
0.8
0.0
saline
HDM
*
*
E
IL-13+ (%)
8
6
4
2
0
saline
HDM
**
**
400 IU
1000 IU
4000 IU
F gated on CD4+
day3
day2
day1
naïve
isotype
Aiolos- PE
G
vehicle
calcitriol
44.7
75.6
Aiolos- PE
CD4 PerCP-eF710
Aiolos+ (%)
100
75
50
25
0
**
WT- vehicle
WT-calcitriol
H
vehicle
calcitriol
WT
Ikzf3-/-
12
4.1
33.6
20.3
IL-2 PE-TexasRed
CD4 PerCP-eF710
IL-2+ (%)
(normalized to vehicle)
****
****
****
WT + vehicle
WT + calcitriol
Ikzf3-/- + vehicle
Ikzf3-/- + calcitriol

Figure 5

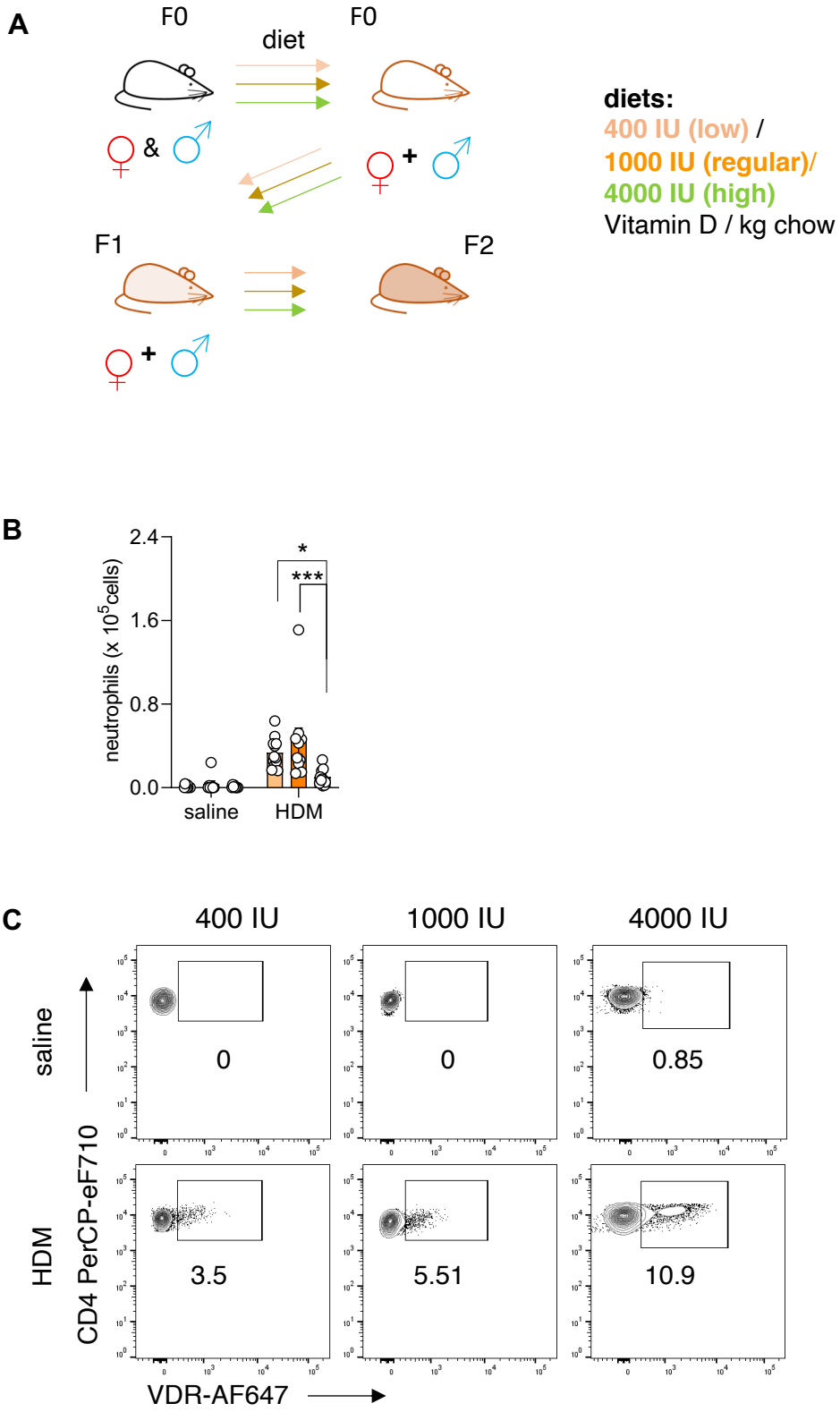

Figure 5 - figure supplement 1

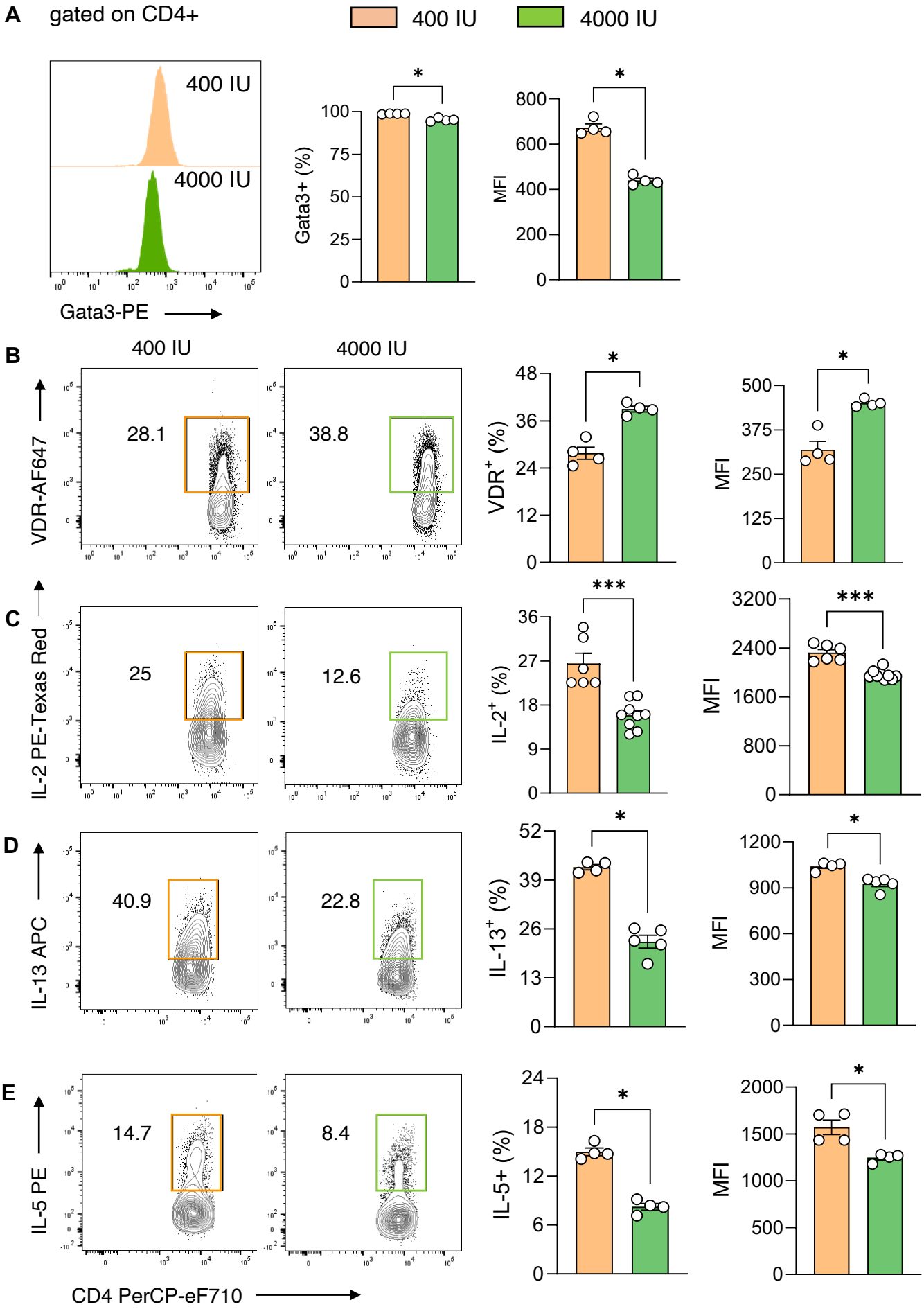

Figure 5 - figure supplement 2

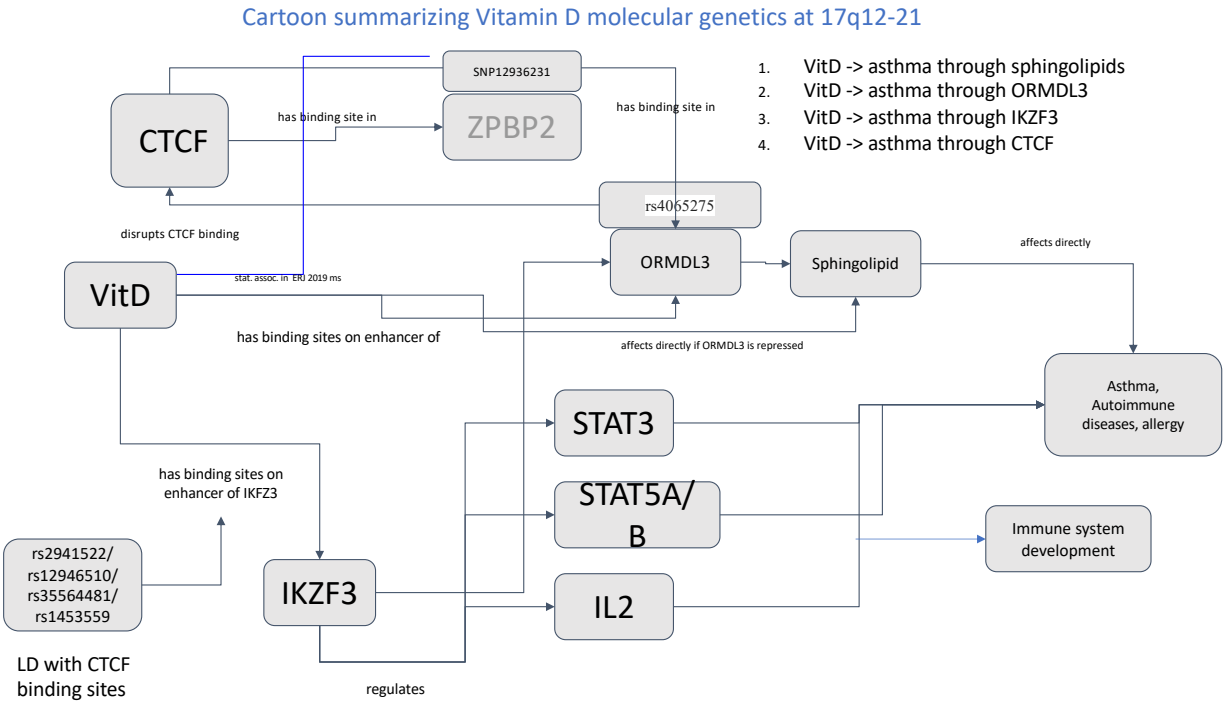

Figure 5 - figure supplement 3

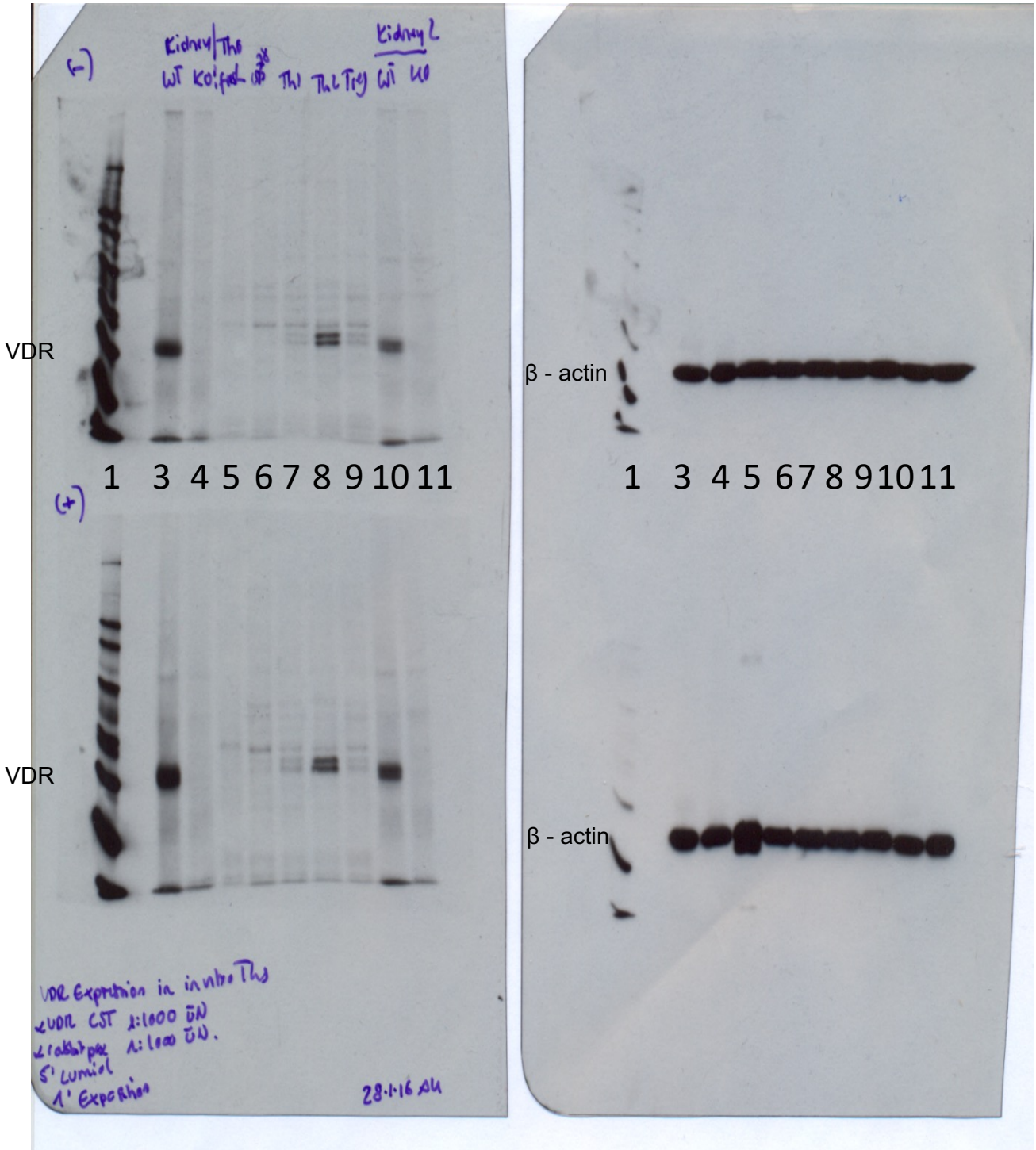

Loading order:
1- marker
2- empty
3- WT kidney sample: positive control
4- VDR-/- kidney sample: negative control
5- CD4+ CD62L+CD44- naïve T cells fresh
6- Th0 cells (24 h CD3 & CD28 stimulation)
7- in vitro Th1
8- in vitro Th2
9- in vitro iTreg
10- WT kidney sample: positive control
11- VDR-/- kidney sample: negative control

Source data-Figure 2 - figure supplement 2A

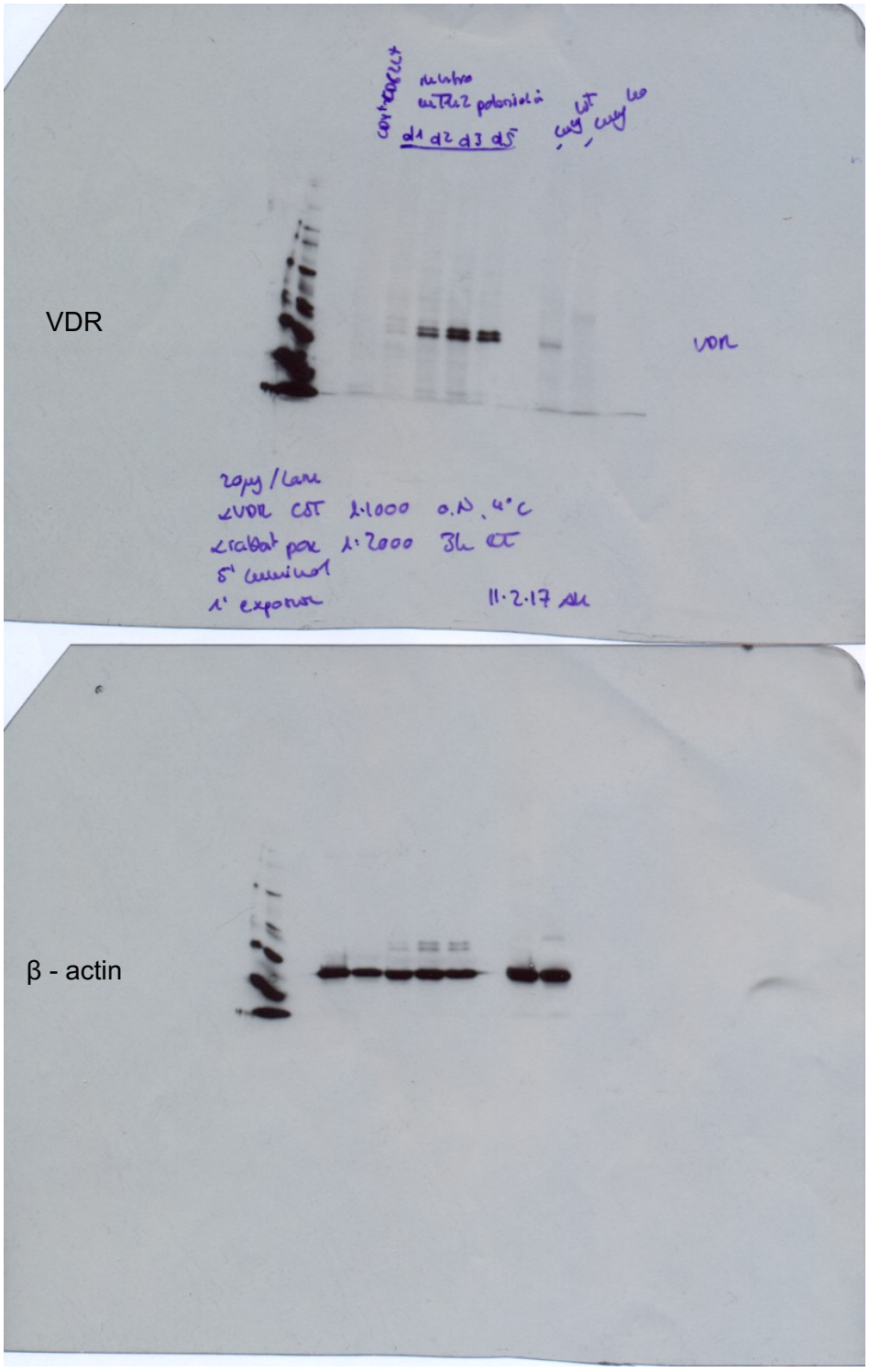

Loading order:
1- marker
2- empty
3- CD4+ CD62L+CD44- naïve T cells fresh
4- in vitro differentiating Th2 day 1
5- in vitro differentiating Th2 day 2
6- in vitro differentiating Th2 day 3
7- in vitro differentiating Th2 day 5
8- empty
9- WT lung sample: positive control
10- VDR-/- lung sample: negative control

Source data-Figure 2 - figure supplement 2B